Supplementary Information for

Crystallization-Driven Template Autocatalysis Induces Mirror Symmetry Breaking and Amplification

Huimin Wu, Qingxuan Chen, Duan Gao, and Zhen Chen

To whom correspondence should be addressed:
zhen.chen@sz.tsinghua.edu.cn (Z.C.)

This PDF file includes:

1. Supplementary Methods
2. Supplementary Notes 1 and 2
3. Supplementary Figures 1−33
4. Supplementary Tables 1−5
5. Captions of Supplementary Videos 1−5
6. Supplementary References 1−4

1. Supplementary Methods

Synthesis of 2,5-dioxopyrrolidin-1-yl 3,4,5-trialkyloxybenzoates

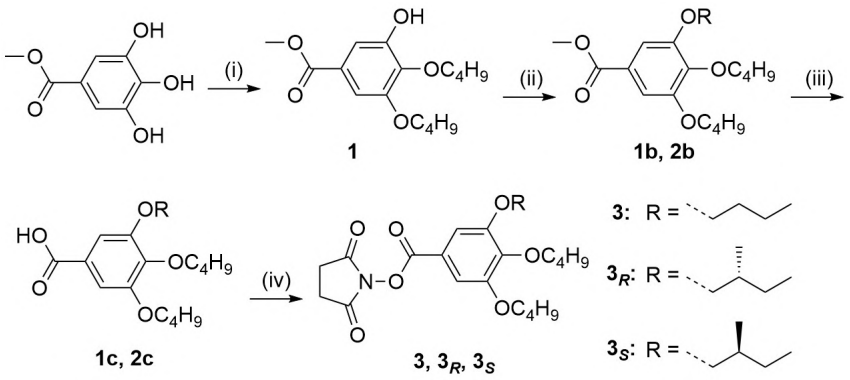

Reagents and conditions: (i) 1-bromobutane, K_2CO_3, DMF, 60 °C; (ii) (*R*)-1-bromo-2-methylbutane or (*S*)-1-iodo-2-methylbutane, K_2CO_3, DMF, 60 °C; (iii) EtOH, H_2O, KOH, 110 °C; (iv) NHS, DCC, 1,4-dioxane, r.t.

Compound 1: In a 300 mL round-bottomed flask, methyl 3,4,5-trihydroxybenzoate (3.40 g, 20 mmol) and anhydrous K_2CO_3 (5.53 g, 40 mmol) were taken and dissolved in 50 mL of dry DMF. The mixture was heated and stirred at 60 °C for 1.5 h. Subsequently, 1-bromobutane (5.48 g, 40 mmol) was added and the mixture was stirred for 20 h at 60 °C. The mixture was poured in 100 mL of water and extracted with ethyl acetate. The organic layer was washed with brine solution (2 × 50 mL), dried over anhydrous $MgSO_4$ and the solution was evaporated using a rotary evaporator. The crude product obtained was purified by column chromatography (silica gel, hexane/ethyl acetate = 80∶1–10∶1) to obtain compound **1** as a white solid in a yield of 90% (5.33 g, 18 mmol). ^{1}H NMR (600 MHz, $CDCl_3$) δ (ppm) = 7.28 (d, J = 1.9 Hz, 1H, Ph-*H*), 7.17 (d, J = 1.9 Hz, 1H, Ph-*H*), 5.88 (s, 1H, O*H*), 4.17 (t, J = 6.7 Hz, 2H, CH_2), 4.03 (t, J = 6.4 Hz, 2H, CH_2), 3.87 (s, 3H, CH_3), 1.85–1.78 (m, 2H, CH_2), 1.77–1.69 (m, 2H, CH_2), 1.55–1.43 (m, 4H, CH_2), 0.98 (dt, J = 12.3, 7.4 Hz, 6H, CH_3). ^{13}C NMR (151 MHz, $CDCl_3$) δ (ppm) = 166.81 (Ph-*C*O), 151.30 (*Ph*-O), 149.17 (*Ph*-OH), 138.66 (*Ph*-O), 125.25 (*Ph*-CO), 109.41 (*Ph*), 106.45 (*Ph*), 73.31 (*C*H_2O), 68.57 (*C*H_2O), 52.14 (*C*H_3O), 32.25 (*C*H_2), 31.30 (*C*H_2), 19.34 (*C*H_2), 19.14 (*C*H_2), 13.83 (*C*H_3), 13.82 (*C*H_3). HR-ESI MS (*m/z*): $[M + H]^+$ calcd. for $C_{16}H_{25}O_5$ 297.16; found: 297.16.

Compound 1b: In a 300 mL round-bottomed flask, compound **1** (5.9 g, 20 mmol) and anhydrous K_2CO_3 (2.76 g, 22 mmol) were taken and dissolved in 50 mL of dry DMF. The mixture was heated and stirred at 60 °C for 1.5 h. Subsequently, (*R*)-1-bromo-2-methylbutane (3.62 g, 24 mmol) was added and the mixture was stirred for 20 h at 60 °C. The mixture was poured in 100 mL of water and extracted with ethyl acetate. The organic layer was washed with brine solution (2 × 50 mL), dried over anhydrous $MgSO_4$ and the solution was evaporated using a rotary evaporator. The crude product obtained was purified by column chromatography (silica gel, hexane/ethyl acetate = 80∶1) to obtain compound **1b** as colorless oil in a yield of 88% (6.44 g, 17.6 mmol). ^{1}H NMR (600 MHz, $CDCl_3$) δ (ppm) = 7.25 (d, J = 1.8 Hz, 2H, Ph-*H*), 4.01 (td, J = 6.5, 3.9 Hz, 4H, OCH_2), 3.88 (s, 3H, CH_3), 3.87–3.84 (m, 1H, OCH_2CH), 3.79 (dd, J = 8.9, 6.5 Hz, 1H, OCH_2CH), 1.90 (dq, J = 13.1, 6.5 Hz, 1H, CH_2CHCH_3), 1.82–1.76 (m, 2H, CH_2),

1.75–1.69 (m, 2H, CH_2), 1.58 [ddd, J = 13.3, 7.5, 5.6 Hz, 1H, CH(CH_3)CH_2], 1.51 (ddt, J = 10.6, 7.4, 3.3 Hz, 4H, CH_2), 1.33–1.26 [m, 1H, CH(CH_3)CH_2], 1.03 (d, J = 6.7 Hz, 3H, CH_3), 0.99–0.92 (m, 9H, CH_3). ^{13}C NMR (151 MHz, $CDCl_3$) δ (ppm) = 166.98 (Ph-*C*O), 153.02 (*Ph*-O), 152.86 (*Ph*-O), 142.33 (*Ph*-O), 124.69 (*Ph*-CO), 107.90 (*Ph*), 107.87 (*Ph*), 73.92 (*C*H_2O), 73.15 (*C*H_2O), 68.83 (*C*H_2O), 52.12 (*C*H_3O), 34.85(CH$_2$*C*HCH$_3$), 32.39 (*C*H_2), 31.37 (*C*H_2), 26.15 (*C*H_2), 19.28 (*C*H_2), 19.19 (*C*H_2), 16.62 (*C*H_3), 13.91 (*C*H_3), 13.85 (*C*H_3), 11.33 (*C*H_3). HR-ESI MS (*m/z*): $[M + H]^+$ calcd. for $C_{21}H_{35}O_5$ 367.24; found: 367.24.

Compound 2b: The similar procedure as above was followed using (*S*)-1-iodo-2-methylbutane. The crude product was purified by column chromatography (silica gel, hexane/ethyl acetate = 80:1) to obtain **2b** as colorless oil in a yield of 80% (5.86 g, 16 mmol). ^{1}H NMR (600 MHz, $CDCl_3$) δ (ppm) = 7.25 (d, J = 1.8 Hz, 2H, Ph-*H*), 4.01 (td, J = 6.5, 3.9 Hz, 4H, OCH_2), 3.88 (s, 3H, CH_3), 3.87–3.84 (m, 1H, OCH_2CH), 3.79 (dd, J = 8.9, 6.5 Hz, 1H, OCH_2CH), 1.90 (dq, J = 13.1, 6.5 Hz, 1H, CH$_2$C*H*CH$_3$), 1.82–1.76 (m, 2H, CH_2), 1.75–1.69 (m, 2H, CH_2), 1.58 [ddd, J = 13.3, 7.5, 5.6 Hz, 1H, CH(CH_3)CH_2], 1.51 (ddt, J = 10.6, 7.4, 3.3 Hz, 4H, CH_2), 1.33–1.26 [m, 1H, CH(CH_3)CH_2)], 1.03 (d, J = 6.7 Hz, 3H, CH_3), 0.99–0.92 (m, 9H, CH_3). ^{13}C NMR (151 MHz, $CDCl_3$) δ (ppm) = 166.98 (Ph-*C*O), 153.02 (*Ph*-O), 152.86 (*Ph*-O), 142.33 (*Ph*-O), 124.69 (*Ph*-CO), 107.90 (*Ph*), 107.87 (*Ph*), 73.92 (*C*H_2O), 73.15 (*C*H_2O), 68.83 (*C*H_2O), 52.12 (*C*H_3O), 34.85(CH$_2$*C*HCH$_3$), 32.39 (*C*H_2), 31.37 (*C*H_2), 26.15 (*C*H_2), 19.28 (*C*H_2), 19.19 (*C*H_2), 16.62 (*C*H_3), 13.91 (*C*H_3), 13.85 (*C*H_3), 11.33 (*C*H_3). HR-ESI MS (*m/z*): $[M + H]^+$ calcd. for $C_{21}H_{35}O_5$ 367.24; found: 367.24.

Compound 1c: In a general procedure, compound **1b** (5.5 g, 15 mmol) and KOH aqueous solution (1.0g, 18 mmol) were dissolved in distilled ethanol (60 mL) and refluxed at 110 °C in a 250 mL round bottom flask for 12 h. After checking the completion of the reaction by TLC, the reaction mixture was then cooled to room temperature, and the solvent was removed under reduced pressure. Then, the reaction mixture was acidified (pH = 2) with cold dilute HCl with continuous stirring and was extracted using ethyl acetate. The organic layer was washed with brine thrice, dried over anhydrous $MgSO_4$, and the filtrate was concentrated under reduced pressure. The product formed was used for the next step without further purification. The crude product obtained was **1c** as a white solid in a yield of 90% (4.75 g, 13.5 mmol). ^{1}H NMR (600 MHz, $CDCl_3$) δ (ppm) = 7.37 (d, J = 1.2 Hz, 2H, Ph-*H*), 4.09 (dt, J = 11.4, 6.5 Hz, 4H, Ph-OCH_2), 3.93 (dd, J = 8.9, 5.9 Hz, 1H, Ph-OCH_2CH), 3.86 (dd, J = 8.9, 6.5 Hz, 1H, Ph-OCH_2CH), 2.01–1.93 (m, 1H, CH$_2$C*H*CH$_2$), 1.85 (dq, J = 7.9, 6.5 Hz, 2H, CH_2), 1.79 (dq, J = 7.9, 6.5 Hz, 2H, CH_2), 1.69–1.61 [m, 1H, CH(CH_3)CH_2], 1.57 (hd, J = 7.4, 2.3 Hz, 4H, CH_2), 1.38–1.32 [m, 1H, CH(CH_3)CH_2], 1.09 (d, J = 6.8 Hz, 3H, CH_3), 1.06–0.97 (m, 9H, CH_3). ^{13}C NMR (151 MHz, $CDCl_3$) δ (ppm) = 171.88 (Ph-*C*O), 153.06 (*Ph*-O), 152.91 (*Ph*-O), 143.16 (*Ph*-O), 123.66 (*Ph*-CO), 108.50 (*Ph*), 108.48 (*Ph*), 73.96 (*C*H_2O), 73.24 (*C*H_2O), 68.88 (*C*H_2O), 34.83 (CH$_2$*C*HCH$_3$), 32.40 (*C*H_2), 31.34 (*C*H_2), 26.17 (*C*H_2), 19.29 (*C*H_2), 19.19 (*C*H_2), 16.63 (*C*H_3), 13.92 (*C*H_3), 13.87 (*C*H_3), 11.34 (*C*H_3). HR-ESI MS (*m/z*): $[M + H]^+$ calcd. for $C_{20}H_{33}O_5$ 353.22; found: 353.23.

Compound 2c: The reaction and work-up procedures were followed similarly to that for com pound **1c**. The product formed was used for the next step without further purification. The crude product, compound **2c**, was obtained as a white solid in a yield of 92% (4.86 g, 13.8 mmol). ^{1}H

NMR (600 MHz, $CDCl_3$) δ (ppm) = 7.37 (d, *J* = 1.2 Hz, 2H, Ph-*H*), 4.09 (dt, *J* = 11.4, 6.5 Hz, 4H, Ph-OCH_2), 3.93 (dd, *J* = 8.9, 5.9 Hz, 1H, Ph-OCH_2CH), 3.86 (dd, *J* = 8.9, 6.5 Hz, 1H, Ph-OCH_2CH), 2.01–1.93 (m, 1H, CH_2CHCH_2), 1.85 (dq, *J* = 7.9, 6.5 Hz, 2H, CH_2), 1.79 (dq, *J* = 7.9, 6.5 Hz, 2H, CH_2), 1.69–1.61 [m, 1H, $CH(CH_3)CH_2$], 1.57 (hd, *J* = 7.4, 2.3 Hz, 4H, CH_2), 1.38–1.32 [m, 1H, $CH(CH_3)CH_2$], 1.09 (d, *J* = 6.8 Hz, 3H, CH_3), 1.06–0.97 (m, 9H, CH_3). ^{13}C NMR (151 MHz, $CDCl_3$) δ (ppm) = 171.88 (Ph-*C*O), 153.06 (*Ph*-O), 152.91 (*Ph*-O), 143.16 (*Ph*-O), 123.66 (*Ph*-CO), 108.50 (*Ph*), 108.48 (*Ph*), 73.96 (CH_2O), 73.24 (CH_2O), 68.88 (CH_2O), 34.83 (CH_2CHCH_3), 32.40 (CH_2), 31.34 (CH_2), 26.17 (CH_2), 19.29 (CH_2), 19.19 (CH_2), 16.63 (CH_3), 13.92 (CH_3), 13.87 (CH_3), 11.34 (CH_3). HR-ESI MS (*m/z*): $[M + H]^+$ calcd. for $C_{20}H_{33}O_5$ 353.22; found: 353.23.

Compound 3*R*: In an anhydrous 1,4-dioxane solution (20 mL), 3,4,5-tripropoxybenzoic acid **1c** (3.52 g, 10.0 mmol) and DCC (2.27 g, 11.0 mmol) were added to NHS (1.27 g, 11.0 mmol), and the mixture was stirred at room temperature for 4 h. After filtration through celite, the filtrate was poured into water (50 mL) and extracted with ethyl acetate twice (2 × 50 mL). The combined organic extract was washed with brine (30 mL) and dried over $MgSO_4$, then filtered to remove the insoluble fraction, and evaporated to dryness. The crude product obtained was purified by column chromatography (silica gel, hexane/ethyl acetate = 3∶1) to obtain compound **3*R*** as a white solid in a yield of 85% (3.8 g, 8.5 mmol). ^{1}H NMR (600 MHz, $CDCl_3$) δ (ppm) = 7.33 (s, 2H, Ph-*H*), 4.04 (dt, *J* = 28.1, 6.5 Hz, 4H, Ph-OCH_2), 3.87 (dd, *J* = 8.8, 5.9 Hz, 1H, Ph-OCH_2CH), 3.79 (dd, *J* = 8.9, 6.5 Hz, 1H, Ph-OCH_2CH), 2.91 (d, *J* = 16.4 Hz, 4H,CH_2CO), 1.97–1.87 (m, 1H, CH_2CHCH_2), 1.84–1.77 (m, 2H, CH_2), 1.77–1.70 (m, 2H, CH_2), 1.62–1.57 [m, 1H, $CH(CH_3)CH_2$], 1.51 (tdd, *J* = 7.4, 5.9, 4.3 Hz, 4H, CH_2), 1.34–1.25 [m, 1H, $CH(CH_3)CH_2$], 1.03 (d, *J* = 6.8 Hz, 3H, CHCH_3), 1.01–0.91 (m, 9H, CH_3). ^{13}C NMR (151 MHz, $CDCl_3$) δ (ppm) = 169.38 (N*C*O), 161.75 (Ph-*C*O), 153.29 (*Ph*-O), 153.15 (*Ph*-O), 144.18 (*Ph*-O), 119.12 (*Ph*-CO), 108.91 (*Ph*), 108.87 (*Ph*), 74.04 (Ph-OCH_2), 73.35 (Ph-OCH_2), 68.99 (Ph-OCH_2), 34.80 (CH_2CHCH_3), 32.37 (CH_2), 31.28 (CH_2), 26.13 (CH_2), 25.72 (CH_2), 19.26 (CH_2), 19.15 (CH_2), 16.61 (CH_2), 13.89 (CH_3), 13.84 (CH_3), 11.33 (CH_3). HR-ESI MS (*m/z*): $[M + H]^+$ calcd. for $C_{24}H_{36}NO_7$ 450.24; found: 450.24.

Compound 3*S*: The reaction and work-up procedures were followed similarly to that for com pound **3*R***. and the crude product obtained was purified by column chromatography (silica gel, hexane/ethyl acetate = 3∶1) to obtain compound **3*S*** as a white solid in a yield of 80% (3.6 g, 8.0 mmol). ^{1}H NMR (600 MHz, $CDCl_3$) δ (ppm) = 7.33 (s, 2H, Ph-*H*), 4.04 (dt, *J* = 28.1, 6.5 Hz, 4H, Ph-OCH_2), 3.87 (dd, *J* = 8.8, 5.9 Hz, 1H, Ph-OCH_2CH), 3.79 (dd, *J* = 8.9, 6.5 Hz, 1H, Ph-OCH_2CH), 2.91 (d, *J* = 16.4 Hz, 4H,CH_2CO), 1.97–1.87 (m, 1H, CH_2CHCH_2), 1.84–1.77 (m, 2H, CH_2), 1.77–1.70 (m, 2H, CH_2), 1.62–1.57 [m, 1H, $CH(CH_3)CH_2$], 1.51 (tdd, *J* = 7.4, 5.9, 4.3 Hz, 4H, CH_2), 1.34–1.25 [m, 1H, $CH(CH_3)CH_2$], 1.03 (d, *J* = 6.8 Hz, 3H, CHCH_3), 1.01–0.91 (m, 9H, CH_3). ^{13}C NMR (151 MHz, $CDCl_3$) δ (ppm) = 169.38 (N*C*O), 161.75 (Ph-*C*O), 153.29 (*Ph*-O), 153.15 (*Ph*-O), 144.18 (*Ph*-O), 119.12 (*Ph*-CO), 108.91 (*Ph*), 108.87 (*Ph*), 74.04 (Ph-OCH_2), 73.35 (Ph-OCH_2), 68.99 (Ph-OCH_2), 34.80 (CH_2CHCH_3), 32.37 (CH_2), 31.28 (CH_2), 26.13 (CH_2), 25.72 (CH_2), 19.26 (CH_2), 19.15 (CH_2), 16.61 (CH_2), 13.89 (CH_3), 13.84 (CH_3), 11.33 (CH_3). HR-ESI MS (*m/z*): $[M + H]^+$ calcd. for $C_{24}H_{36}NO_7$ 450.24; found: 450.24.

Synthesis of 6,7-dithionaphthalonitrile precursors

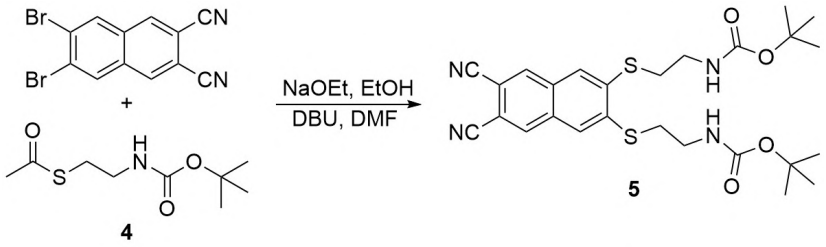

Compound 5: To an ethanol solution (20 mL) of compound **4** (1 g, 4.5 mmol), sodium ethoxide (340 mg, 5.00 mmol) was added under a nitrogen atmosphere at 25 ºC. The mixture was stirred for 1 h. The reaction mixture was then evaporated to dryness under reduced pressure. To the residue was added a DMF (20 mL) solution of 2,3-dibromo-6,7-dicyanonaphthalene (670 mg, 2.0 mmol) and DBU (760 mg, 5.0 mmol), the resulting mixture was stirred at 20 ºC for 4 h. Afterward, water (50 mL) was added to the reaction mixture, and the forming white precipitate was collected by filtration. The crude solid was purified via column chromatography (silica gel, CH_2Cl_2/ethyl acetate = 10∶1) to yield compound **5** as a white solid in a yield of 36% (230 mg, 0.75 mmol). ^{1}H NMR (600 MHz, DMSO-d_6) δ (ppm) = 8.57 (s, 2H, Ph-*H*), 8.05 (s, 2H, Ph-*H*), 7.13 (t, J = 5.7 Hz, 2H), 3.29–3.23 (m, 4H, CH_2NH), 3.20 (t, J = 6.3 Hz, 4H, PhSCH_2), 1.38 (s, 18H, CH_3). ^{13}C NMR (151 MHz, DMSO-d_6) δ (ppm) = 156.07 (NH*C*O), 141.06 (*Ph*), 135.28(*Ph*-S), 131.15(*Ph*), 124.06 (*Ph*), 117.06 (*C*N), 108.40 (*Ph*-CN), 78.49 (O*C*H), 38.96 (*C*H_2NH), 32.21 (PhS*C*H_2), 28.69 (*C*H_3). HR-ESI MS (*m/z*): $[M + H]^+$ calcd. for $C_{26}H_{33}N_4O_4S_2$ 529.19; found: 529.19.

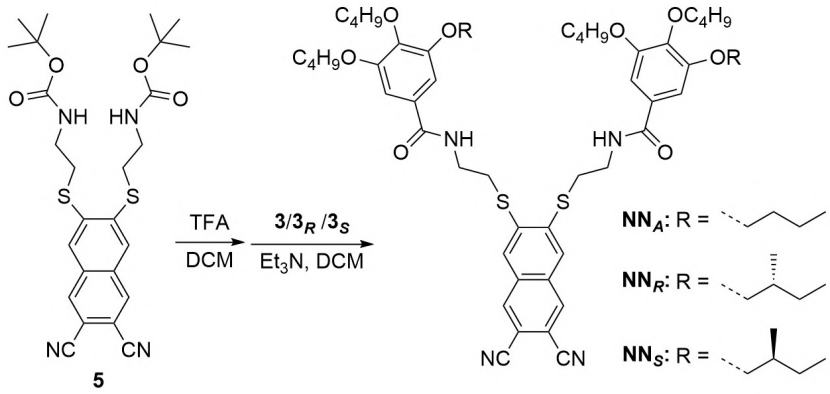

NN$_A$: Compound **5** (0.50 g, 0.94 mmol) was dissolved in CH_2Cl_2 and chilled in an ice bath. TFA (3 mL) was then added dropwise to the solution, which was stirred at 25 °C for 2 h. The reaction mixture was evaporated to dryness under reduced pressure. A mixture of compound **3** (1.35 g, 3.10 mmol) and Et_3N (6 mL) in 10 mL of CH_2Cl_2 was then added to the residue. The mixture was stirred at room temperature for 12 h. The resulting solution was evaporated to dryness and then separated in MeOH. The precipitate was filtered off, yielding **NN**$_A$ (0.52 g, 0.54 mmol) as a white powder in 58% yield. ^{1}H NMR (600 MHz, $CDCl_3$) δ (ppm) = 8.19 (s, 2H, Ph-*H*), 8.04 (s, 2H, Ph-*H*), 6.92 (s, 4H, Ph-*H*), 6.79 (t, J = 6.0 Hz, 2H, N*H*CO), 3.97 (dt, J = 19.9, 6.5 Hz, 12H, Ph-OCH_2), 3.68 (q, J = 6.5 Hz, 4H, CH_2NH), 3.36 (t, J = 6.8 Hz, 4H, PhSCH_2), 1.75 (dddd, J = 32.4, 12.4, 8.9, 6.5 Hz, 12H, CH_2), 1.49 (dp, J = 14.8, 7.5 Hz, 12H,

C*H*$_2$), 0.96 (td, *J* = 7.4, 3.9 Hz, 18H, C*H*$_3$). ^{13}C NMR (151 MHz, $CDCl_3$) δ (ppm) = 167.80 (NH*C*O), 153.09 (*Ph*-O), 141.51 (*Ph*-O), 140.62 (*Ph*), 134.49 (*Ph*-S), 131.30 (*Ph*), 128.46 (*Ph*), 126.0 (*Ph*-CO), 115.91 (*C*N), 109.77 (*Ph*-CN), 105.74 (*Ph*), 73.20 (Ph-O*C*H$_2$), 69.12 (Ph-O*C*H$_2$), 39.35 (*C*H$_2$NH), 32.31 (PhS*C*H$_2$), 32.03 (*C*H$_2$), 31.38 (*C*H$_2$), 19.27 (*C*H$_2$), 19.15 (*C*H$_2$), 13.89 (*C*H$_3$), 13.85 (*C*H$_3$). HR-ESI MS (*m/z*): $[M + H]^+$ calcd. for $C_{54}H_{73}N_4O_8S_2$ 969.48; found: 969.48.

NN$_R$: Using a similar procedure to that for **NN$_A$**, **NN$_R$** was synthesized and obtained in a yield of 55% (0.51 g, 0.52 mmol) from **3$_R$** (1.40 g, 3.10 mmol). ^{1}H NMR (600 MHz, $CDCl_3$) δ (ppm) = 8.19 (s, 2H, Ph-*H*), 8.05 (s, 2H, Ph-*H*), 6.96–6.87 (m, 4H, Ph-*H*), 6.81 (t, *J* = 6.1 Hz, 2H, N*H*CO), 3.96 (dt, *J* = 18.6, 6.5 Hz, 8H, Ph-OC*H*$_2$), 3.80 (dd, *J* = 8.8, 5.9 Hz, 2H, Ph-OC*H*$_2$CH(CH$_3$)), 3.76–3.72 [m, 2H, Ph-OC*H*$_2$CH(CH$_3$)], 3.69 (q, *J* = 8.0, 6.5 Hz, 4H, C*H*$_2$NH), 3.36 (t, *J* = 6.9 Hz, 4H, PhSC*H*$_2$), 1.87 [dt, *J* = 13.0, 6.5 Hz, 2H, CH$_2$C*H*(CH$_3$)], 1.81–1.68 (m, 8H, C*H*$_2$), 1.59–1.45 (m, 10H, C*H*$_2$), 1.30–1.21 [m, 2H, CH(CH$_3$)C*H*$_2$], 1.01 (d, *J* = 6.8 Hz, 6H, C*H*$_3$), 0.97–0.91 (m, 18H, C*H*$_3$). ^{13}C NMR (151 MHz, $CDCl_3$) δ (ppm) = 167.81 (NH*C*O), 153.21 (*Ph*-O), 153.08 (*Ph*-O), 141.26 (*Ph*-O), 140.49 (*Ph*), 134.48 (*Ph*-S), 131.23 (*Ph*), 128.42 (*Ph*), 125.81 (*Ph*-CO), 115.94 (*C*N), 109.66 (*Ph*-CN), 105.46 (*Ph*), 105.37 (*Ph*), 74.03 (Ph-O*C*H$_2$), 73.19 (Ph-O*C*H$_2$), 68.97 (Ph-O*C*H$_2$), 39.30 (*C*H$_2$NH), 34.80 (CH$_2$*C*HCH$_3$), 32.32 (PhS*C*H$_2$), 31.81 (*C*H$_2$), 31.33 (*C*H$_2$), 26.08 (*C*H$_2$), 19.26 (*C*H$_2$), 19.16 (*C*H$_2$), 16.58 (*C*H$_3$), 13.92 (*C*H$_3$), 13.87 (*C*H$_3$), 11.35 (*C*H$_3$). HR-ESI MS (*m/z*): $[M + H]^+$ calcd. for $C_{56}H_{77}N_4O_8S_2$ 997.51; found: 997.51.

NN$_S$: Using a similar procedure to that for **NN$_A$**, **NN$_S$** was synthesized and obtained in a yield of 60% (0.56 g, 0.56 mmol) from **3$_S$** (1.40 g, 3.10 mmol). ^{1}H NMR (600 MHz, $CDCl_3$) δ (ppm) = 8.18 (s, 2H, Ph-*H*), 8.05 (s, 2H, Ph-*H*), 6.96–6.88 (m, 4H, Ph-*H*), 6.75 (t, *J* = 6.0 Hz, 2H, N*H*CO), 3.97 (dt, *J* = 19.4, 6.3 Hz, 8H, Ph-OC*H*$_2$), 3.80 [dd, *J* = 8.8, 5.9 Hz, 2H, Ph-OC*H*$_2$CH(CH$_3$)], 3.76–3.72 [m, 2H, Ph-OC*H*$_2$CH(CH$_3$)], 3.69 (q, *J* = 8.0, 6.5 Hz, 4H, C*H*$_2$NH), 3.37 (t, *J* = 6.8 Hz, 4H, PhSC*H*$_2$), 1.93–1.83 [m, 2H, CH$_2$C*H*(CH$_3$)], 1.81–1.68 (m, 8H, C*H*$_2$), 1.52 (ddq, *J* = 22.3, 14.9, 7.1 Hz, 10H, C*H*$_2$), 1.27 (dt, *J* = 14.3, 7.5 Hz, 2H, CH(CH$_3$)C*H*$_2$), 1.02 (dd, *J* = 6.7, 1.1 Hz, 6H, C*H*$_3$), 0.99–0.88 (m, 18H, C*H*$_3$). ^{13}C NMR (151 MHz, $CDCl_3$) δ (ppm) = 167.77 (NH*C*O), 153.26 (*Ph*-O), 153.12 (*Ph*-O), 141.48 (*Ph*-O), 140.58 (*Ph*), 134.46 (*Ph*-S), 131.28 (*Ph*), 128.44 (*Ph*), 126.00 (*Ph*-CO), 115.88 (*C*N), 109.79 (*Ph*-CN), 105.66 (*Ph*), 105.56 (*Ph*), 74.15 (Ph-O*C*H$_2$), 73.21 (Ph-O*C*H$_2$), 69.08 (Ph-O*C*H$_2$), 39.37 (*C*H$_2$NH), 34.85 (CH$_2$*C*HCH$_3$), 32.35 (PhS*C*H$_2$), 31.96 (*C*H$_2$), 31.38 (*C*H$_2$), 26.11, (*C*H$_2$) 19.26 (*C*H$_2$), 19.17 (*C*H$_2$), 16.58 (*C*H$_3$), 13.90 (*C*H$_3$), 13.85 (*C*H$_3$), 11.33 (*C*H$_3$). HR-ESI MS (*m/z*): $[M + H]^+$ calcd. for $C_{56}H_{77}N_4O_8S_2$ 997.51; found: 997.51.

2. Supplementary Notes

Supplementary Note 1 | Analysis of sergeant-and-soldiers experiments

To fit and quantify the data of net helicity η at 680 nm for sergeant-and-soldiers experiments, we employed a modified sergeant-and-soldiers model, which initially developed by van Gestel [1]. The least square method was developed by using the numerical calculation program MATLAB to fit the experimental data, the contour plot of the sum of squares of the residuals shows a narrow area with minimum values at σ and ω are obtained. Subsequently, two types of free energy penalties were measured: the helix reversal penalty (HRP) and the mismatch penalty (MMP) based on two parameters, σ and ω. The σ represents a dimensionless measure of the helix reversal penalty associated with helix reversal, which is related to the helix reversal penalty (HRP) as follows:

$$\sigma = \exp(-\frac{2\mathrm{HRP}}{RT}) \tag{S1}$$

The ω represents a dimensionless measure of the mismatch penalty for a homochiral monomer in a bonded state with the less preferred handedness, which is related to the mismatch penalty (MMP) as follows:

$$\omega = \exp(-\frac{\mathrm{MMP}}{RT}) \tag{S2}$$

The net helicity η of the columns, which can be written as follows:

$$\eta = \frac{z(1-\omega)}{\sqrt{z^2(1-\omega)^2 + 4\sigma(1+z)(1-z\omega)}} \tag{S3}$$

The fraction homochiral material x, which can be written as follows:

$$x = \frac{z\omega}{(1+z\omega)} + \frac{z(1+\eta)(1-\omega)}{(1+z)(1+z\omega)} \tag{S4}$$

In equations S1–S4 the following parameters have been used: where η is the net helicity, z is the excess fugacity of the homochiral component, a measure for its relative abundance in the solution, ω is the dimensionless mismatch penalty; MMP is the mismatch penalty (kJ mol^{-1}). σ is the dimensionless helix reversal penalty; HRP is the helix reversal penalty (kJ mol^{-1}). where R is the ideal gas constant and T is the absolute temperature. x is the enantiomeric excess.

Supplementary Note 2 | Analysis of kinetics in the nucleation stage of CDTA

Time-dependent kinetic data were acquired by monitoring the reaction at a fixed wavelength using a JASCO V-760 UV-Visible spectrophotometer equipped with an INSTEC HCS402 hot stage, where a powdery sample of NN mixed with DCTH was sandwiched between two identical glass plates (18 × 18 mm). The absorbance at 810 nm were subsequently subjected to nonlinear best fitting based on an autocatalytic model[2] using the equation as follows:

$$A = A_\infty + (A_0 - A_\infty)(1 + (m-1)\{k_0 t + (n+1)^{-1}(k_c t)^{n+1}\})^{-1/(m-1)} \qquad \text{(S5)}$$

The parameters subjected to optimization were A, A_0, A_∞, k_0, k_c, m and n, where A, A_0, and A_∞ correspond to the absorbance at an arbitrary time t, at starting time, and at the final stage of the aggregation process, respectively. k_0 is defined as the rate constant for the induction period; k_c is defined as the rate constant for the nucleation stage; m is a parameter representing the size of the critical nucleus; and n is an exponent characterizing the power-law time dependence of CDTA. The corresponding kinetic parameters are summarized in Supplementary Table 5.

3. Supplementary Figures

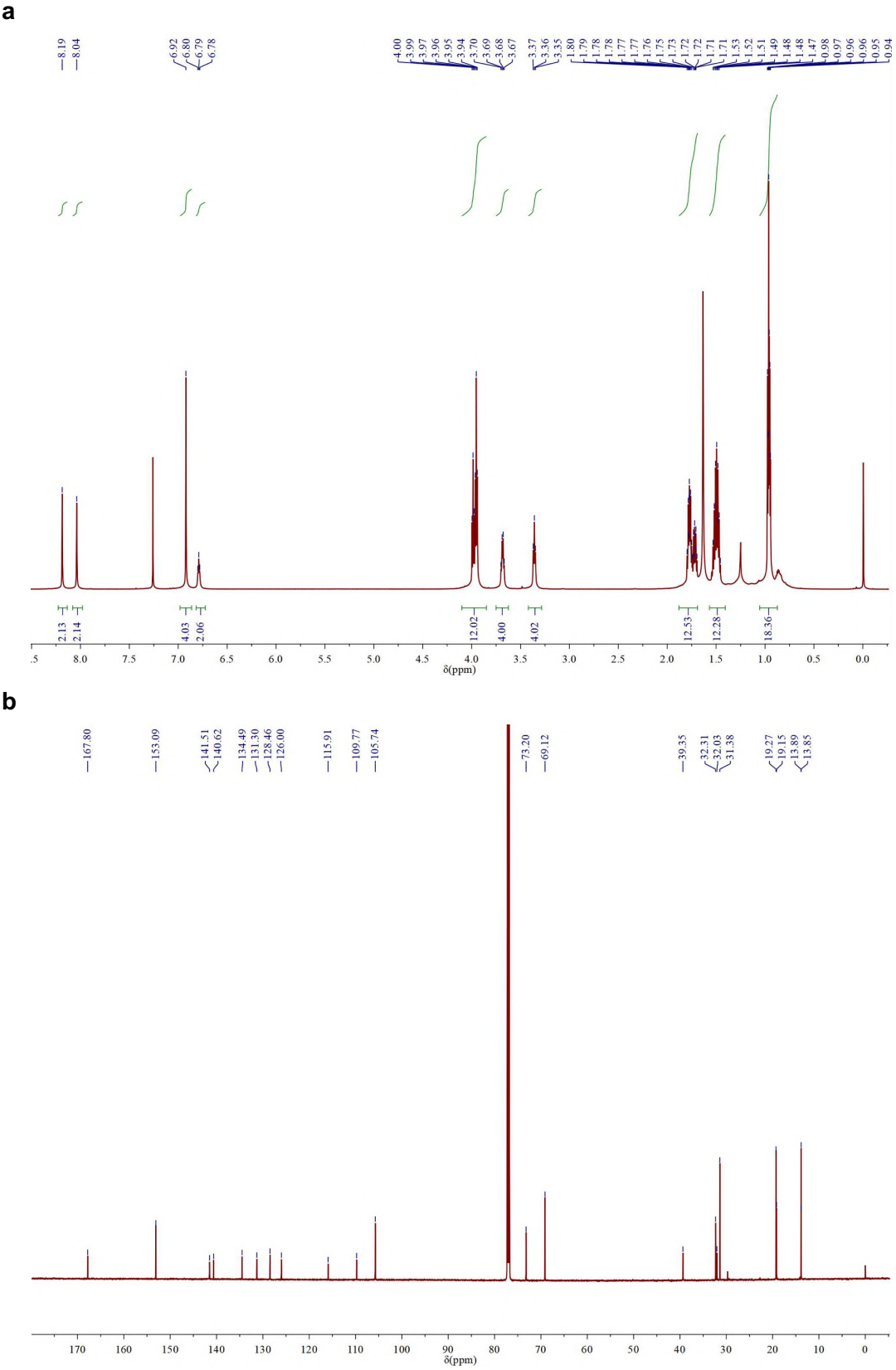

Supplementary Fig. 1 | a,**b**, ^{1}H NMR (**a**) and ^{13}C NMR (**b**) spectra of **NN*A*** in $CDCl_3$ at 25 °C.

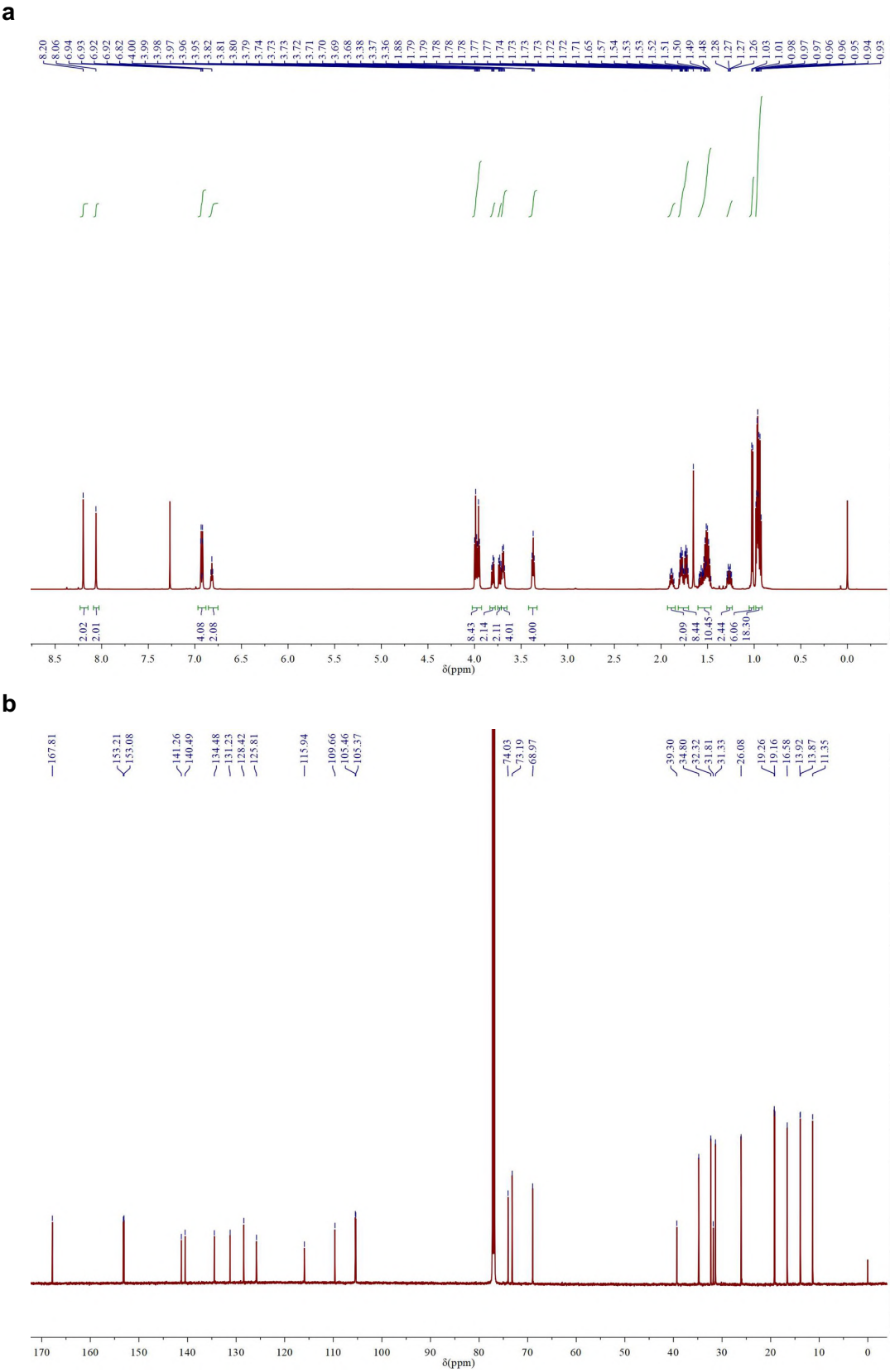

Supplementary Fig. 2 | a,**b**, ^{1}H NMR (**a**) and ^{13}C NMR (**b**) spectra of **NN*R*** in $CDCl_3$ at 25 °C.

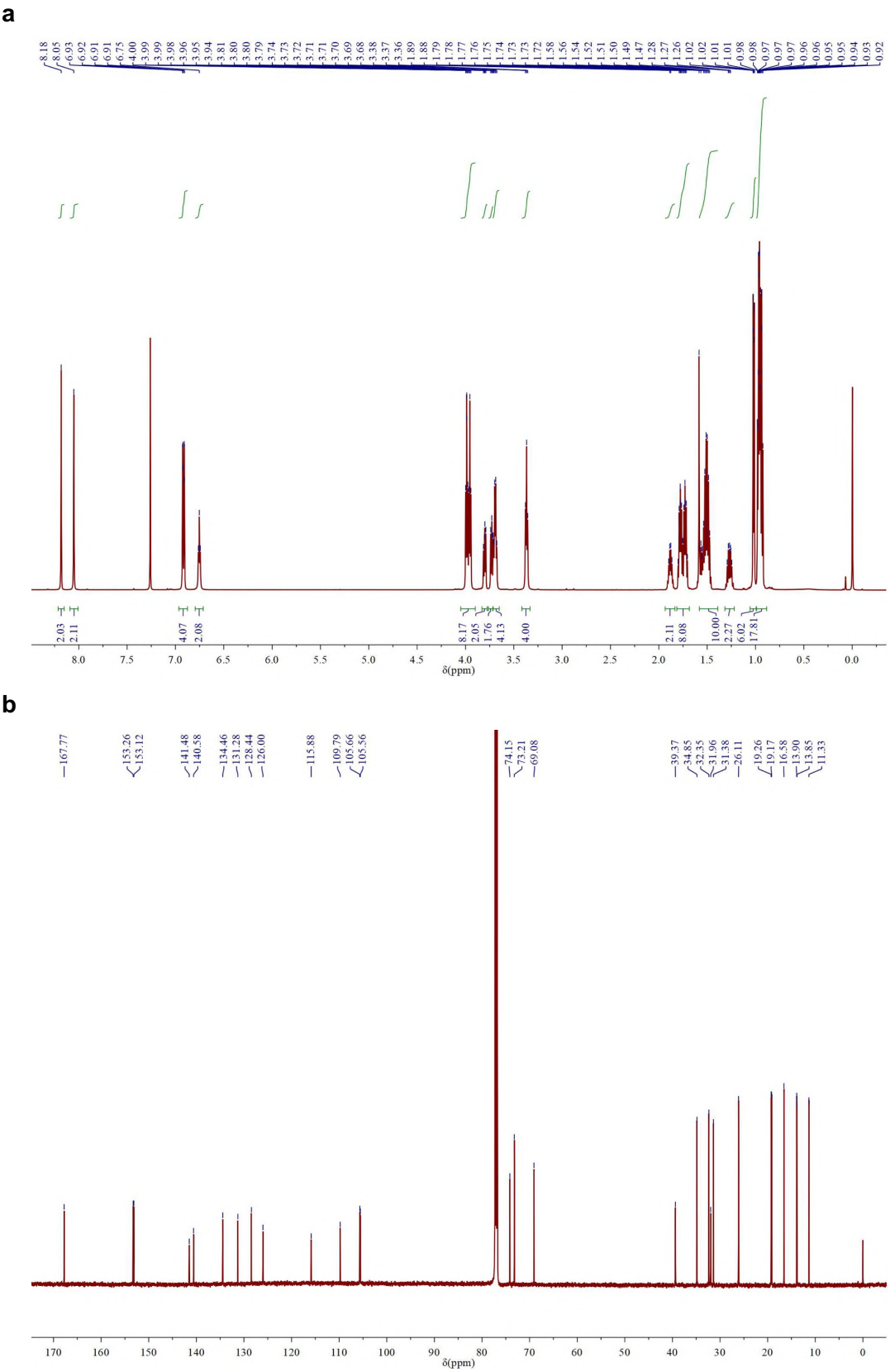

Supplementary Fig. 3 | a,**b**, ^{1}H NMR (**a**) and ^{13}C NMR (**b**) spectra of **NN*S*** in $CDCl_3$ at 25 °C.

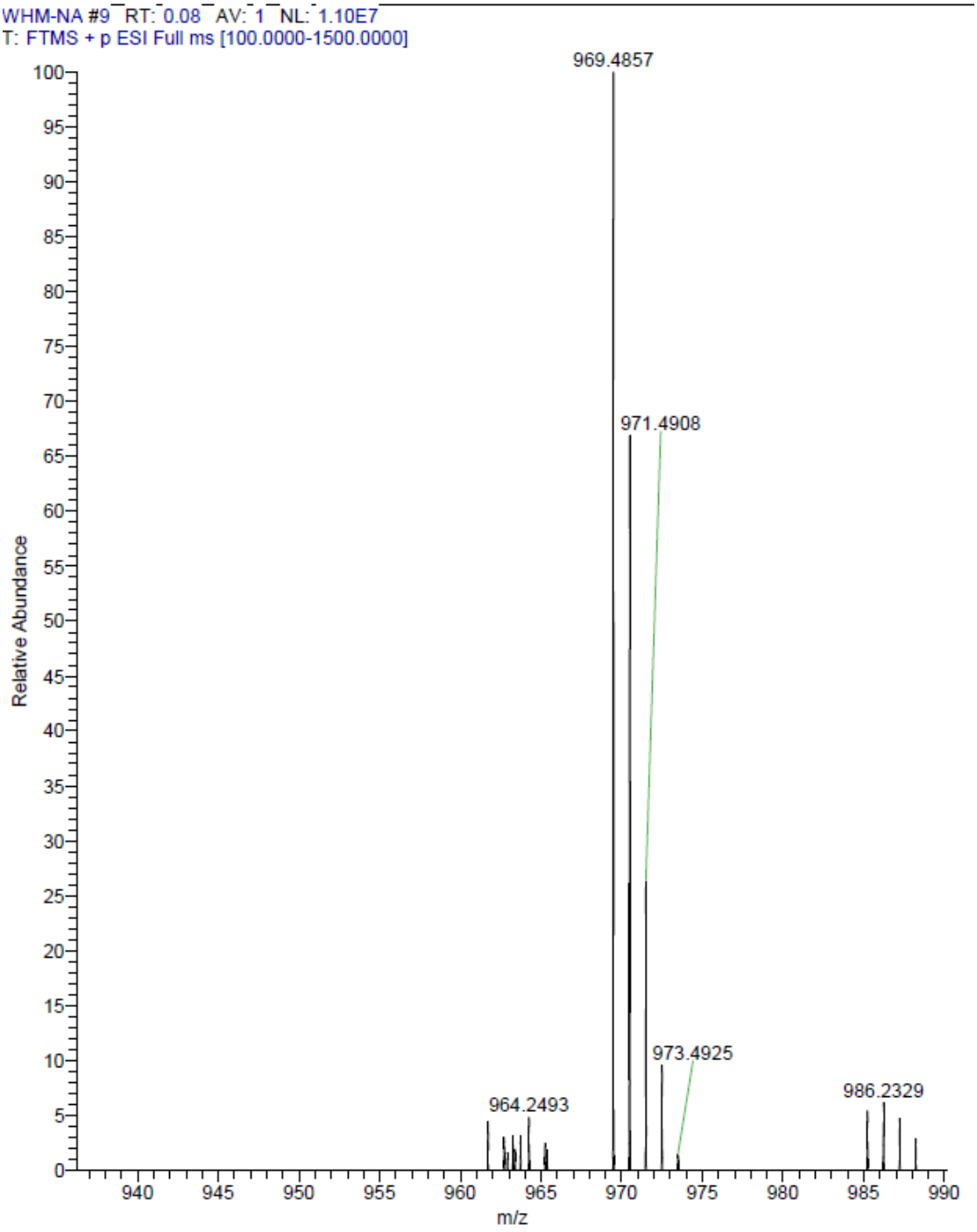

Supplementary Fig. 4 | HR-ESI mass spectrum of **NN**$_A$.

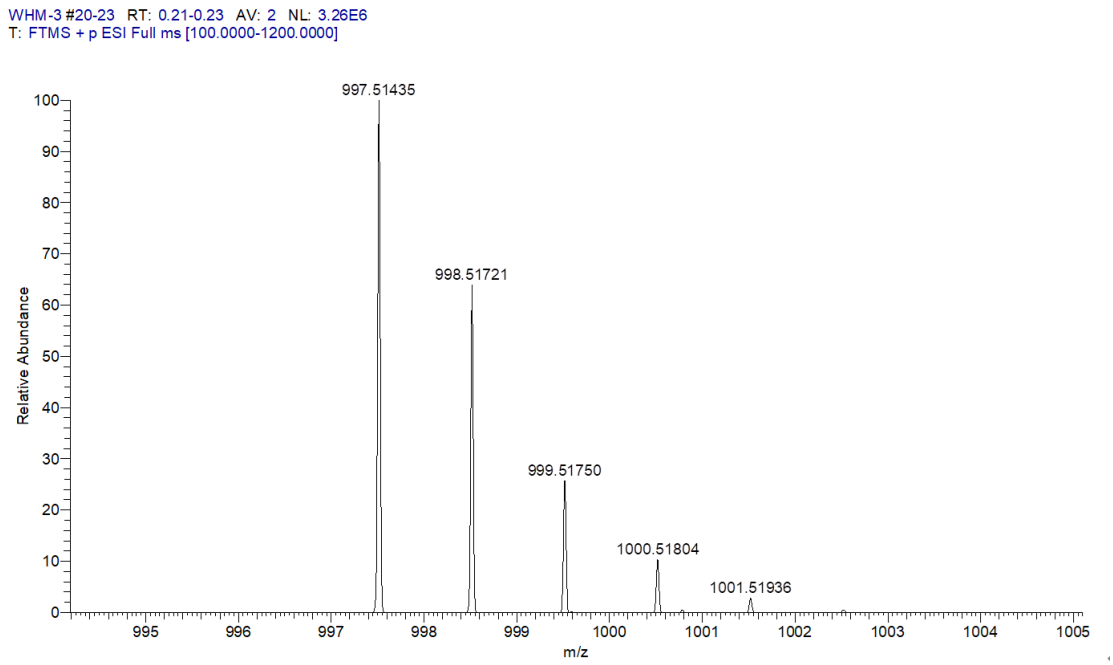

Supplementary Fig. 5 | HR-ESI mass spectrum of **NN**$_{R}$.

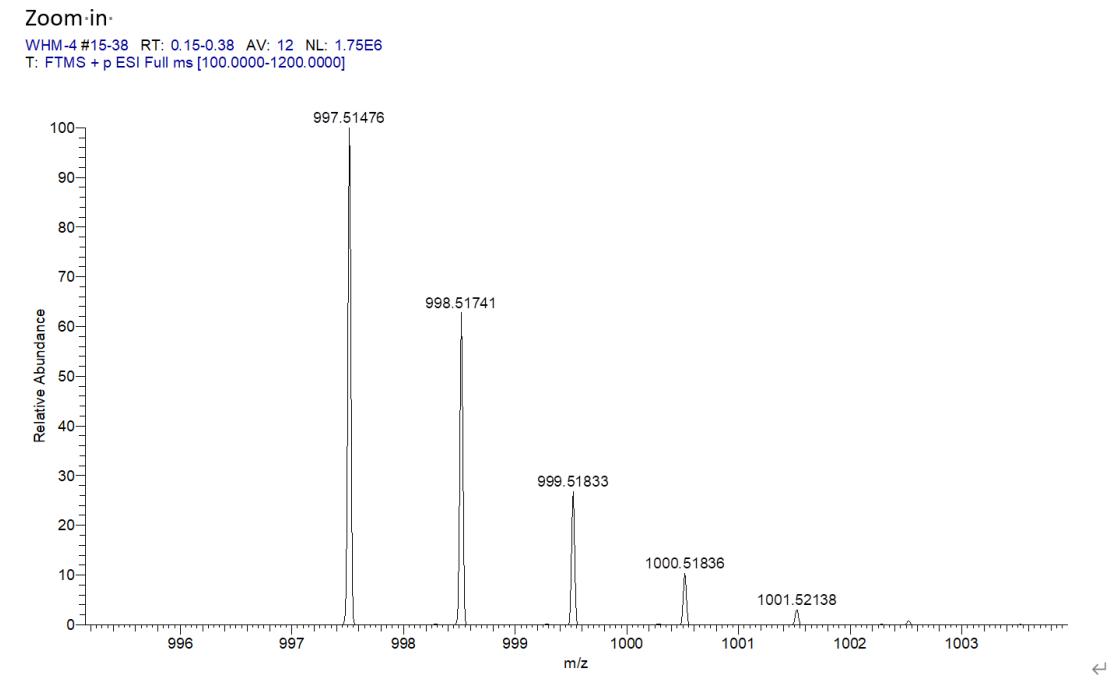

Supplementary Fig. 6 | HR-ESI mass spectrum of **NN**$_{S}$.

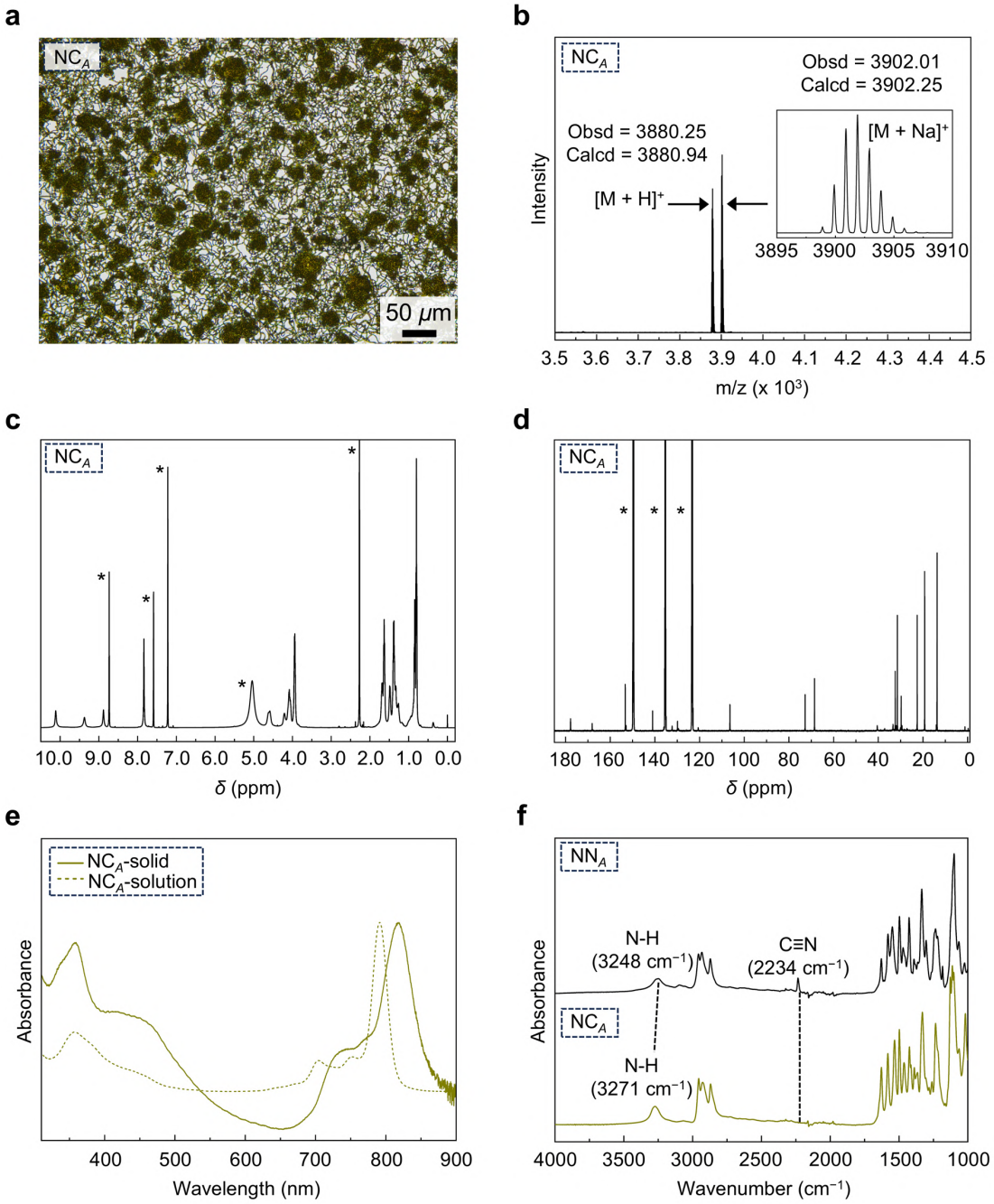

Supplementary Fig. 7 | **a**, OM image of [**NC**$_A$]^{CF} after washing with MeOH at 25 °C. **b**, MALDI-TOF mass spectrum of [**NC**$_A$]^{CF} after washing with MeOH at 25 °C. The inset shows a magnified peak due to [**NC**$_A$]^{CF}. **c**,**d**, ^{1}H NMR (**c**) and ^{13}C NMR (**d**) spectra of [**NC**$_A$]^{CF} dissolved in d^5-pyridine with zinc (II) acetate were recorded at 25 °C. Solvents are marked by (*). **e**, UV–vis absorption spectra of [**NC**$_A$]^{CF} in solid state (straight line) and in pyridine (dashed line). **f**, FT-IR spectra were recorded at 25 °C of **NN**$_A$ (black) and [**NC**$_A$]^{CF} (brown) on KBr planes.

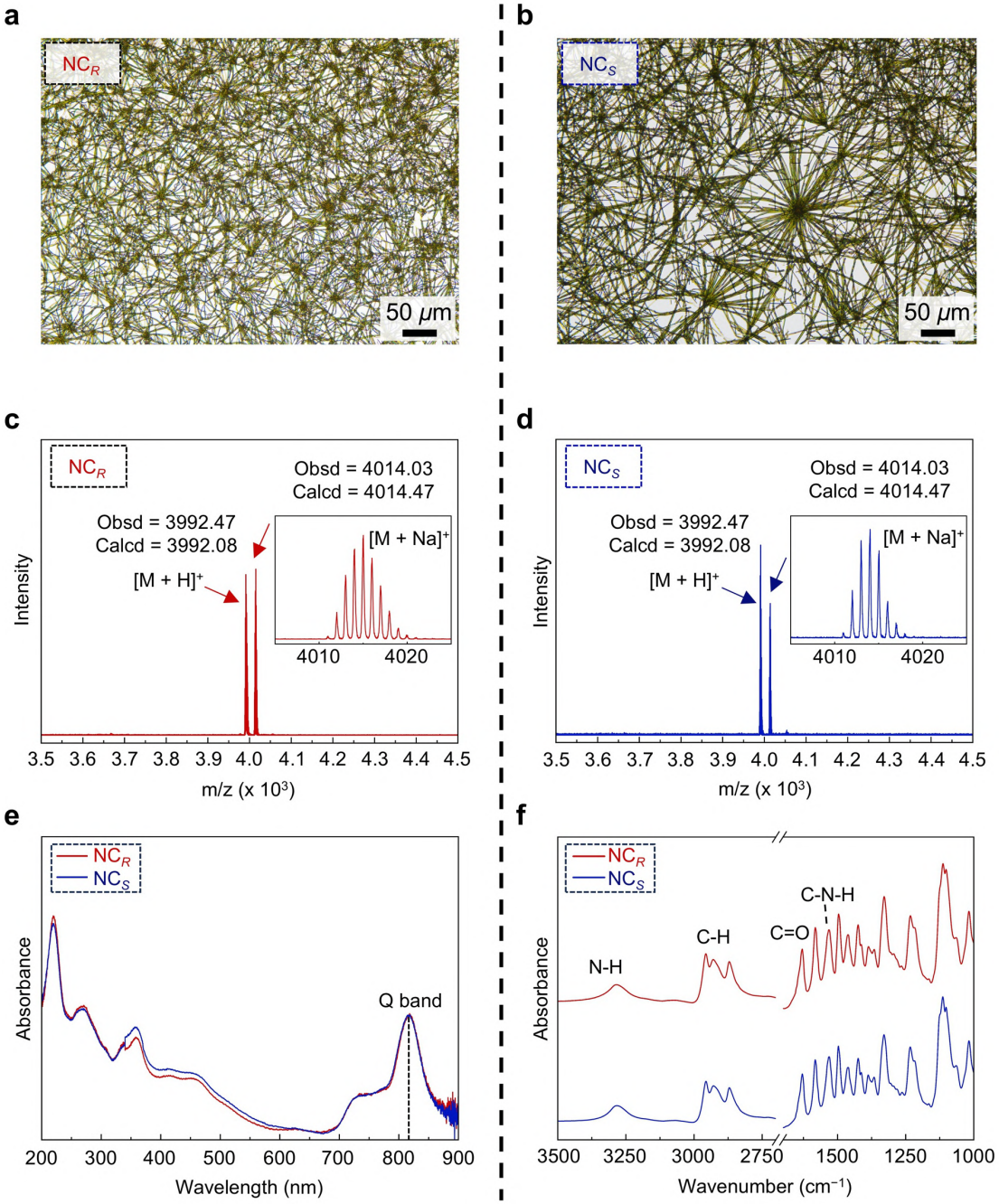

Supplementary Fig. 8 | **a**,**b**, OM images of [**NC*R***]^{CF} (**a**) and [**NC*S***]^{CF} (**b**) after washing with MeOH at 25 °C. **c**,**d**, MALDI-TOF mass spectra of [**NC*R***]^{CF} (**c**) and [**NC*S***]^{CF} (**d**) after washing with MeOH at 25 °C. The inset shows a magnified peak due to [**NC*R***]^{CF} and [**NC*S***]^{CF}. **e**, UV–vis absorption spectra of [**NC*R***]^{CF} (blue) and [**NC*S***]^{CF} (red) in solid state at 25 °C. **f**, FT-IR spectra of [**NC*R***]^{CF} (blue) and [**NC*S***]^{CF} (red) on KBr planes at 25 °C.

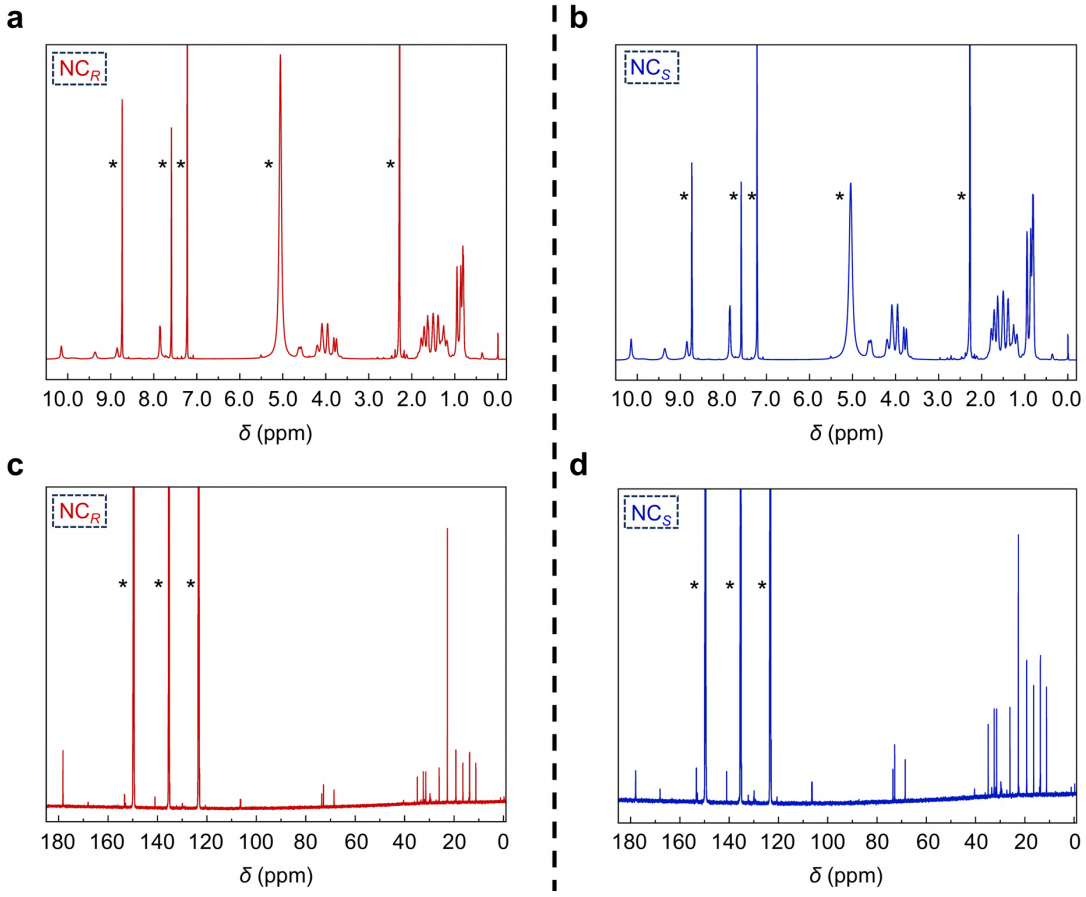

Supplementary Fig. 9 | **a**,**b**, ^{1}H NMR spectra of [**NC*R***]^{CF} (**a**) and [**NC*S***]^{CF} (**b**) dissolved in d^5-pyridine with zinc (II) acetate at 25 °C. Solvents are marked by (*). **c**,**d**, ^{13}C NMR spectra of [**NC*R***]^{CF} (**c**) and [**NC*S***]^{CF} (**d**) dissolved in d^5-pyridine with zinc (II) acetate at 25 °C. Solvents are marked by (*).

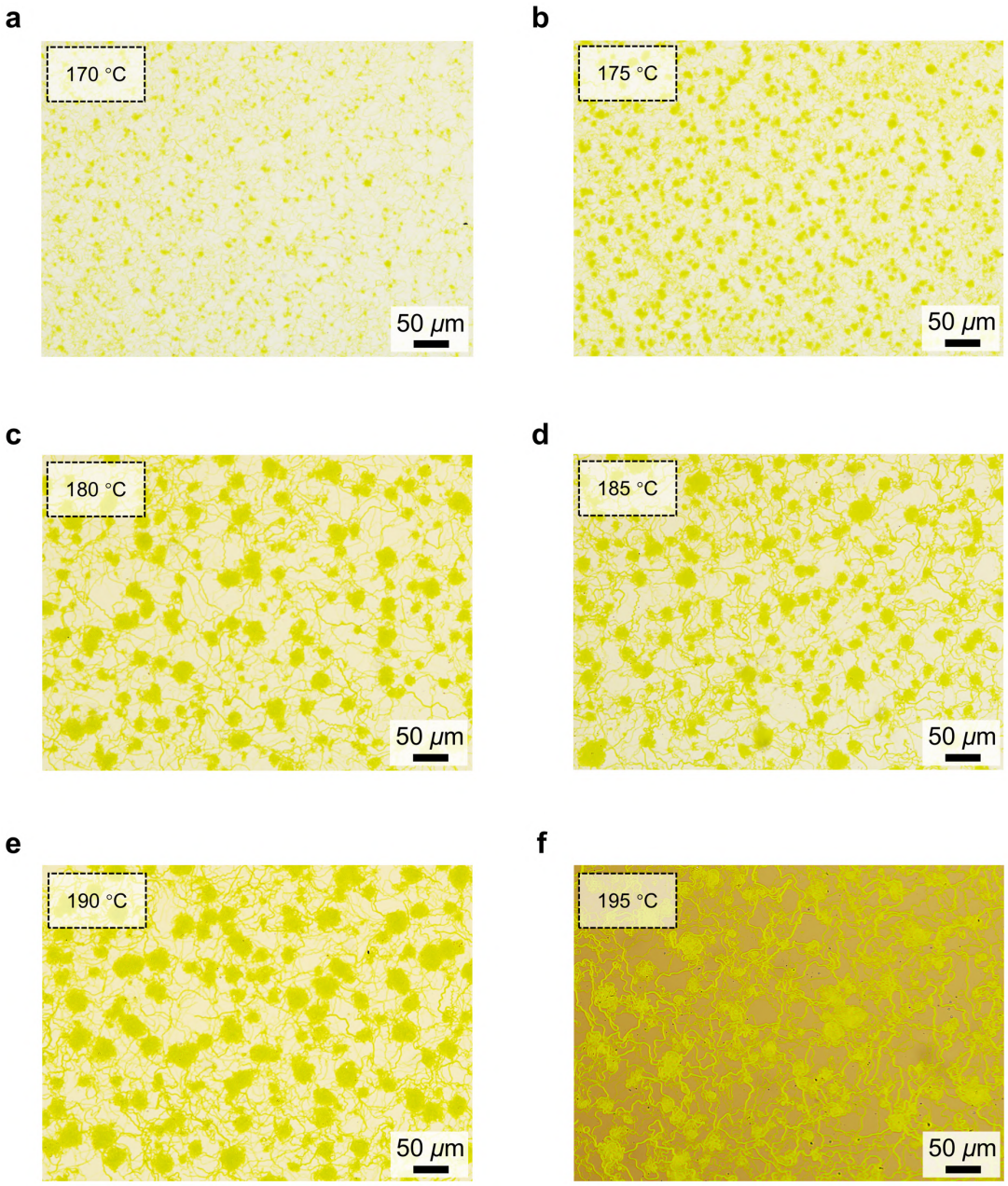

Supplementary Fig. 10 | a–f, OM images of the reaction mixtures obtained by heating $\mathbf{NN}_A$ at 170 °C (**a**), 175 °C (**b**), 180 °C (**c**), 185 °C (**d**), 190 °C (**e**), and 195 °C (**f**) for 12 h.

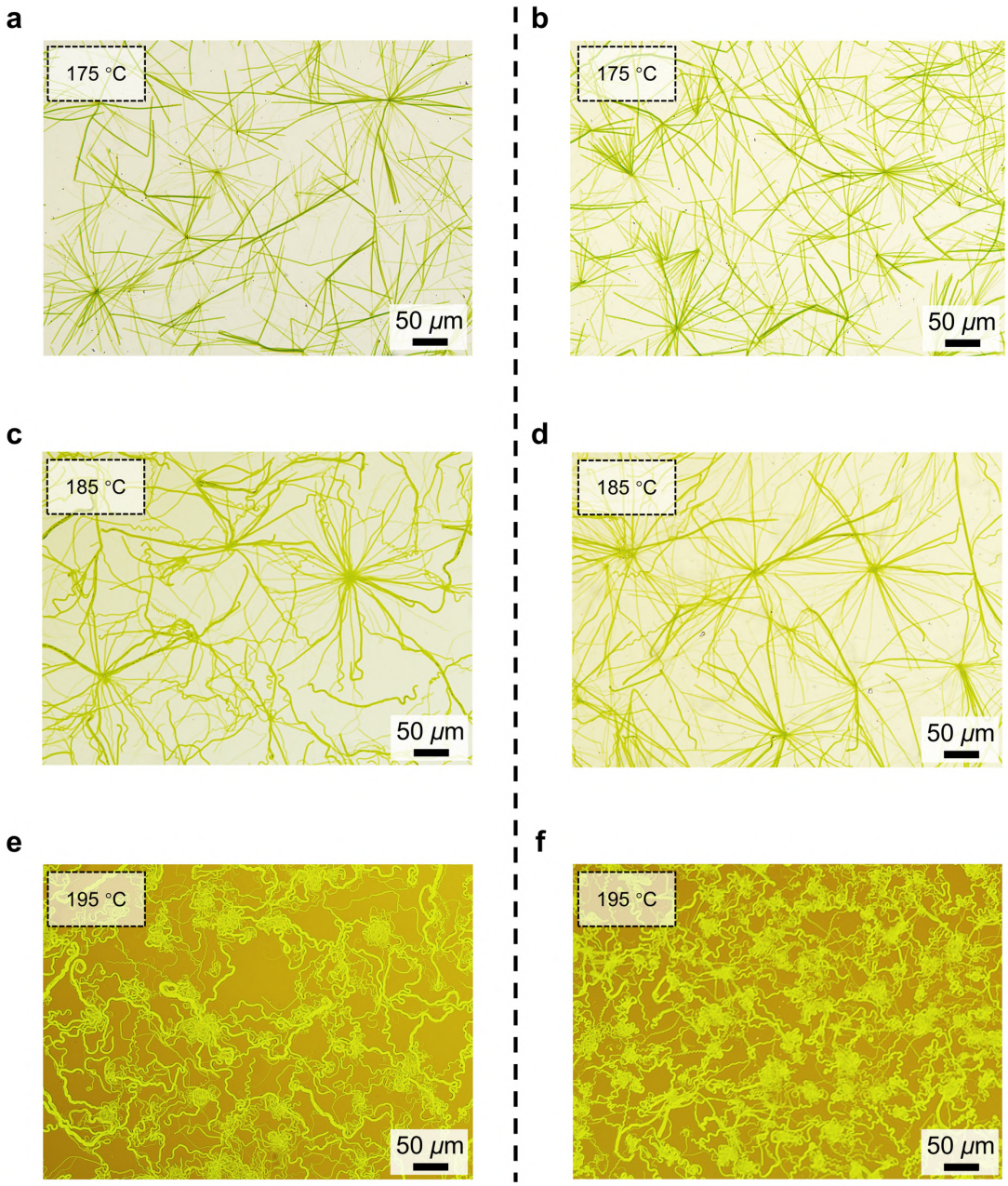

Supplementary Fig. 11 | **a**,**c**,**e**, OM images of the reaction mixtures obtained by heating $\mathbf{NN}_R$ at175 ℃ (**a**), 185 ℃ (**c**), and 195 ℃ (**e**) for 12 h. **b**,**d**,**f**, OM images of the reaction mixtures obtained by heating $\mathbf{NN}_S$ at 175 ℃ (**b**), 185 ℃ (**d**), and 195 ℃ (**f**) for 12 h.

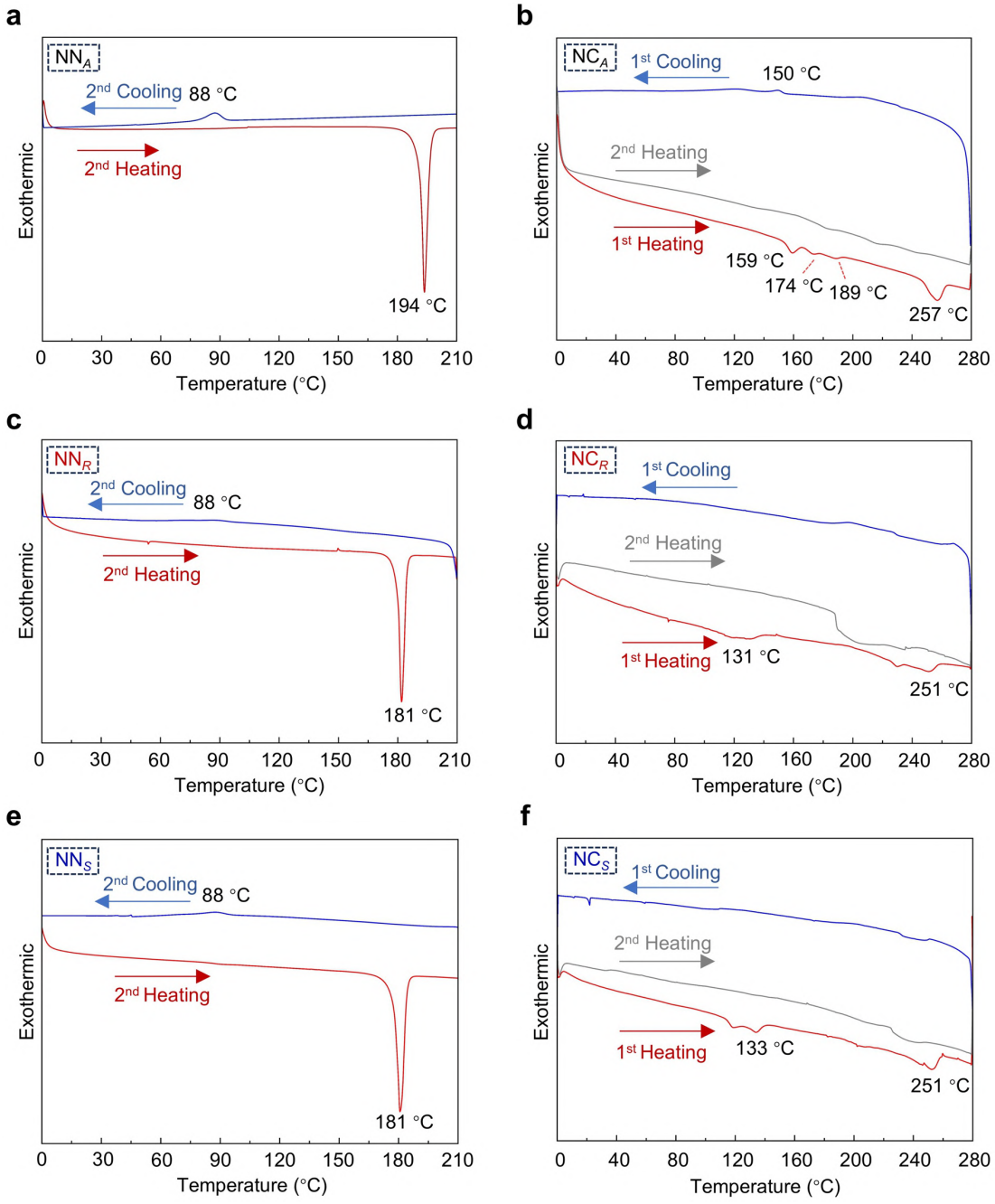

Supplementary Fig. 12 | a–f, DSC traces of **NN$_A$** (**a**) and **NC$_A$** (**b**), **NN$_R$** (**c**) and **NC$_R$** (**d**), **NN$_S$** (**e**) and **NC$_S$** (**f**) on the various heating/cooling cycles at a scan rate of 10 °C min^{-1}. Note that the endothermic signals during the second heating process disappeared due to overheating indicating that the as-formed crystals obtained by CDTA are in a thermodynamically non-equilibrium stationary state.

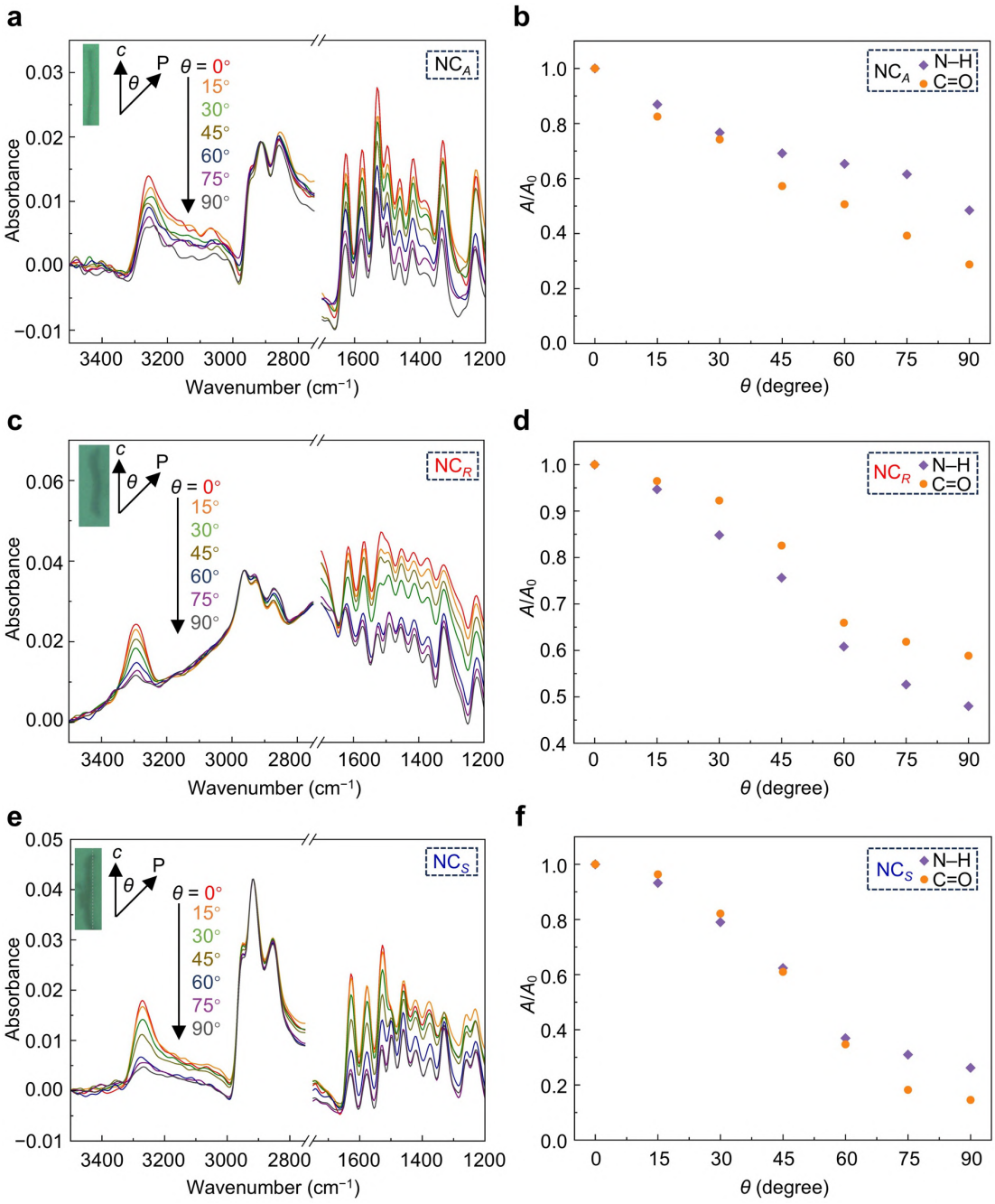

Supplementary Fig. 13 | **a**,**c**,**e**, Polarized FT-IR spectra at different azimuthal angles (θ) from 0° to 90° of [**NC*A***]^{CF} (**a**), [**NC*R***]^{CF} (**c**), and [**NC*S***]^{CF} (**e**) after washing with MeOH at 25 °C. θ is defined as 0° when the polarizing direction of incident light (P) is parallel to the *c* axis of the crystal. **b**,**d**,**f**, Angle-dependent plots of the relative absorption change (A/A_0) at ~3270 cm^{-1} ($\nu_{N–H}$) and ~1620 cm^{-1} ($\nu_{C=O}$) for [**NC*A***]^{CF} (**b**), [**NC*R***]^{CF} (**d**), and [**NC*S***]^{CF} (**f**) recorded upon rotating the polarizer at every 15° intervals.

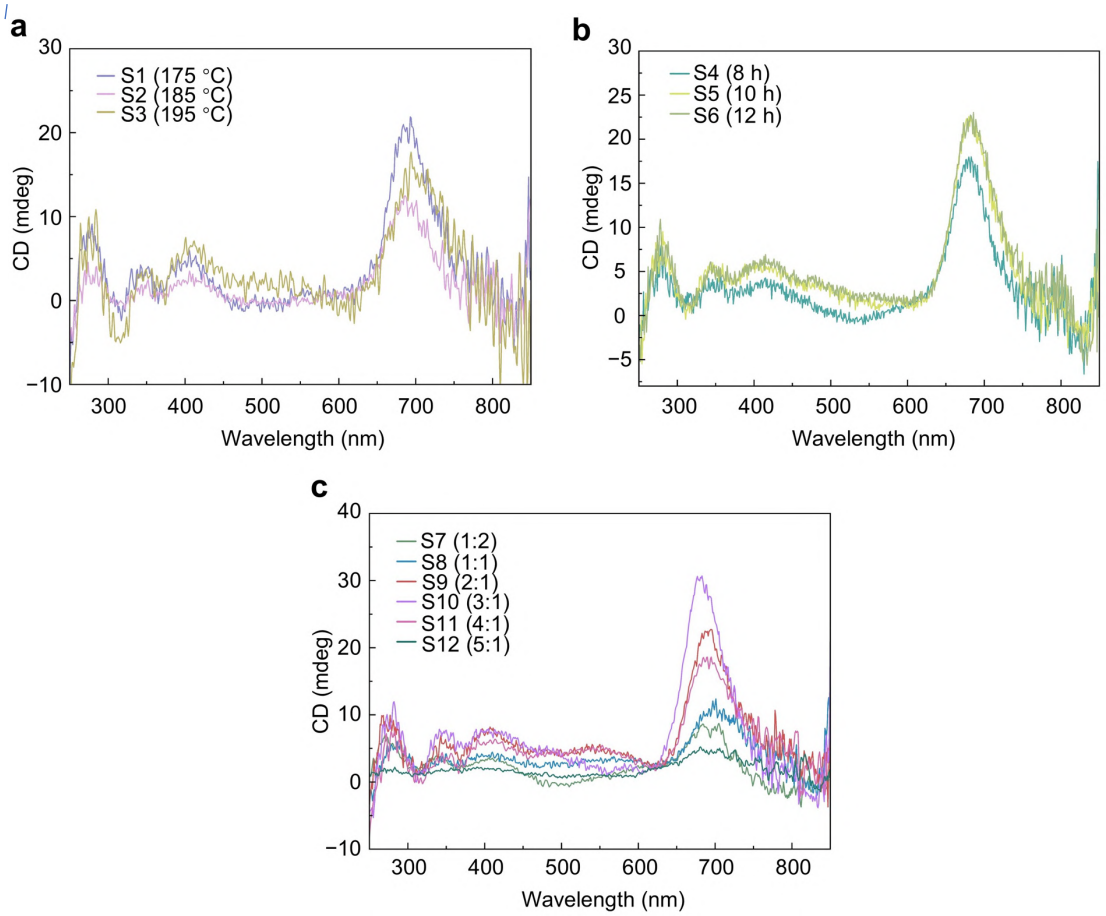

Supplementary Fig. 14 | **a**, CD spectra of the suspensions in $CHCl_3$ of $[\mathbf{NC}_A]^{CF}$ obtained by heating a mixture of $\mathbf{NN}_A$ with DCTH ($[\mathbf{NN}_A]$/[DCTH] = 3:1) at 175 °C, 185 °C, and 195 °C for 12 h. **b**, CD spectra of the suspensions in $CHCl_3$ of $[\mathbf{NC}_A]^{CF}$ obtained by heating $\mathbf{NN}_A$ with DCTH ($[\mathbf{NN}_A]$/[DCTH] = 3:1) at 185 °C for 8 h, 10 h, and 12 h. **c**, CD spectra of the suspensions in $CHCl_3$ of $[\mathbf{NC}_A]^{CF}$ obtained by heating $\mathbf{NN}_A$ at 185 °C for 12 h, premixed with DCTH at molar ratios of 1:2, 1:1, 2:1, 3:1, 4:1, and 5:1.

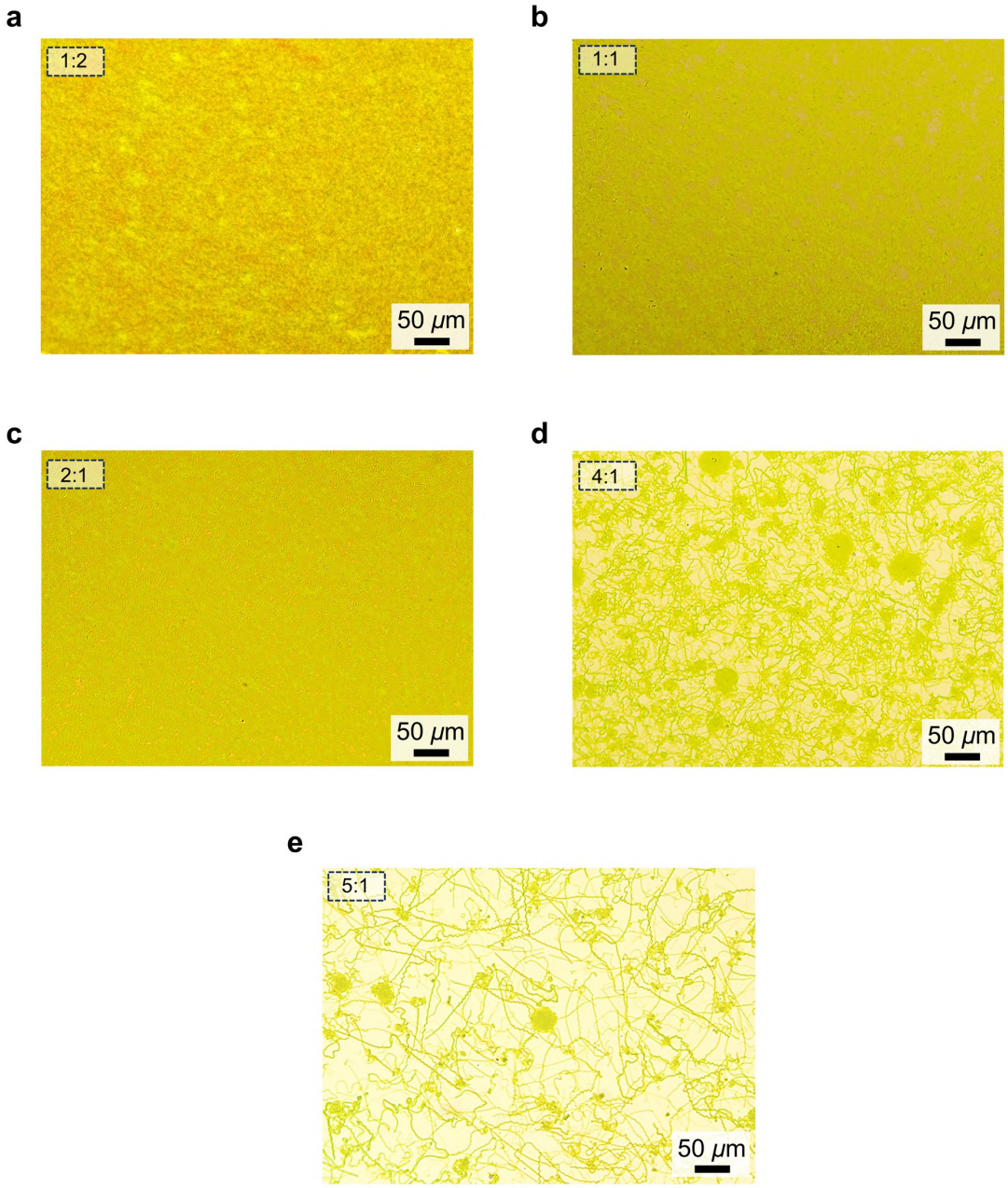

Supplementary Fig. 15 | **a**–**e**, OM images of the reaction mixtures obtained by heating $\mathbf{NN}_A$ premixed with DCTH in molar ratios of 1:2 (**a**), 1:1 (**b**), 2:1 (**c**), 4:1 (**d**), 5:1 (**e**) at 185 °C for 12 h.

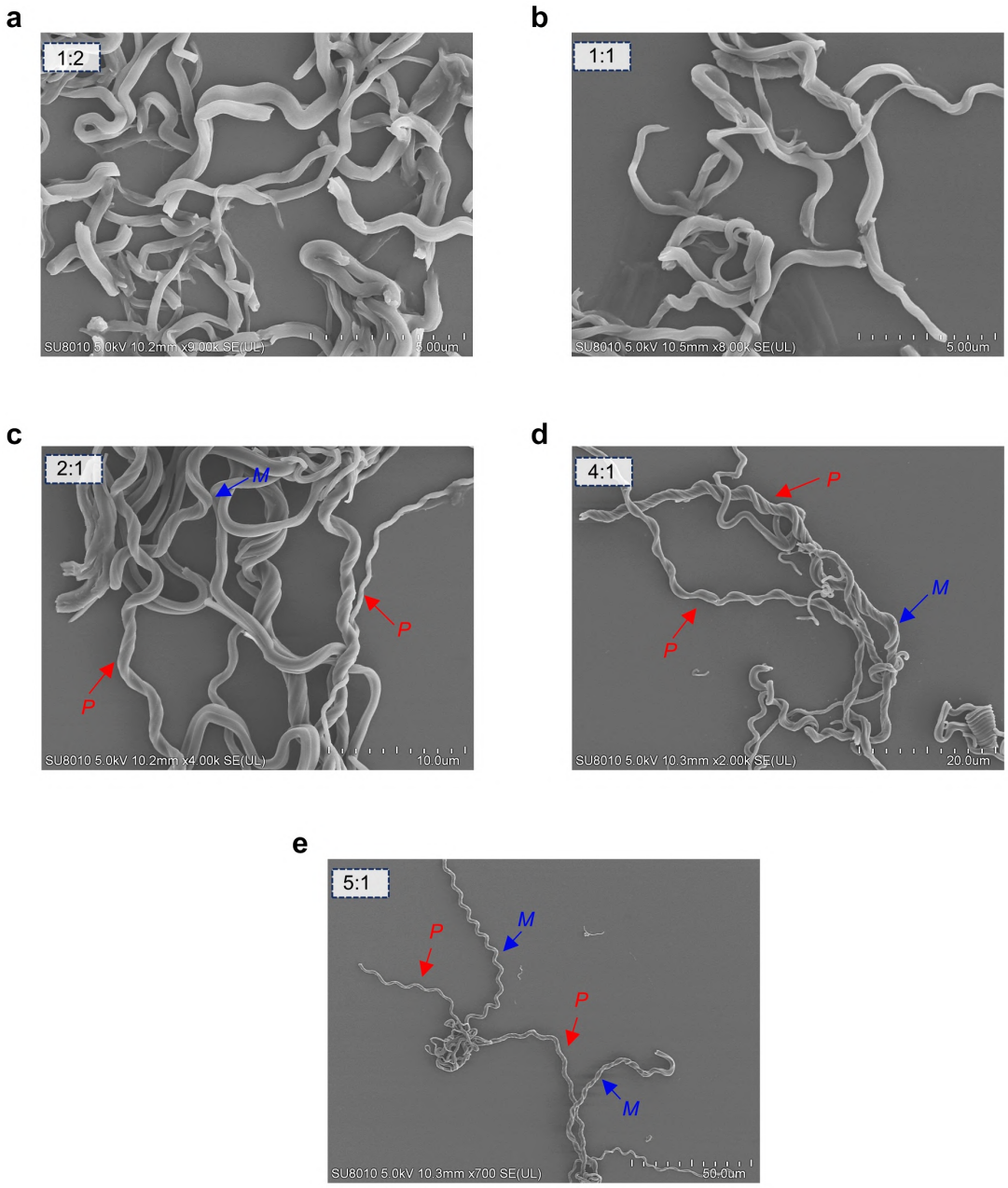

Supplementary Fig. 16 | **a**–**e**, Representative SEM images of the reaction mixtures obtained by heating $\mathbf{NN}_A$ premixed with DCTH in molar ratios of 1:2 (**a**), 1:1 (**b**), 2:1 (**c**), 4:1 (**d**), 5:1 (**e**) at 185 °C for 12 h.

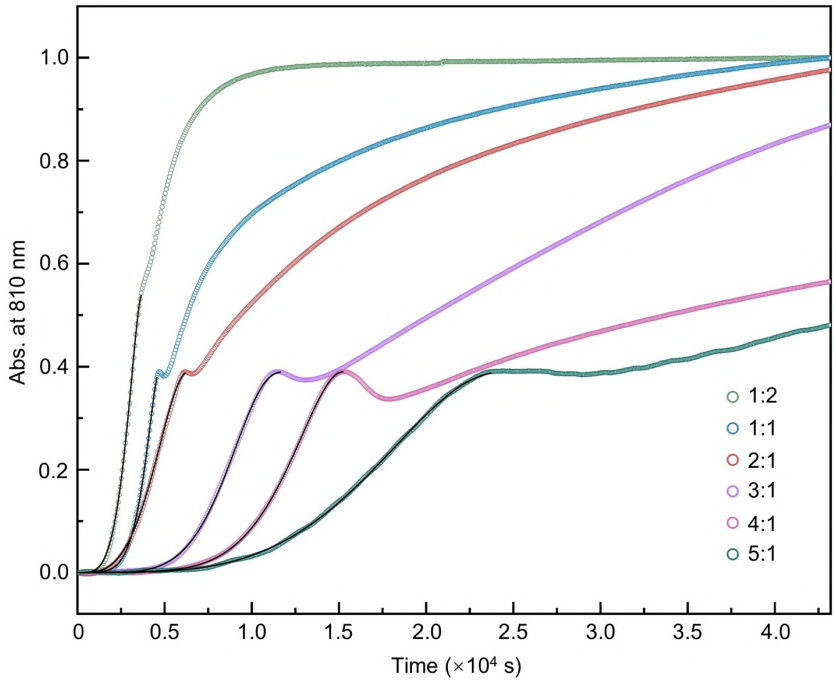

Supplementary Fig. 17 | Kinetic and fit profiles of absorbance for the reaction mixtures obtained by heating $\mathbf{NN}_A$ premixed with DCTH at molar ratios of 1:2, 1:1, 2:1, 3:1, 4:1, 5:1 at 185 °C for 12 h. The solid lines represent the fit (R^2 = 0.999) on an autocatalytic model in the nucleation stage of CDTA.

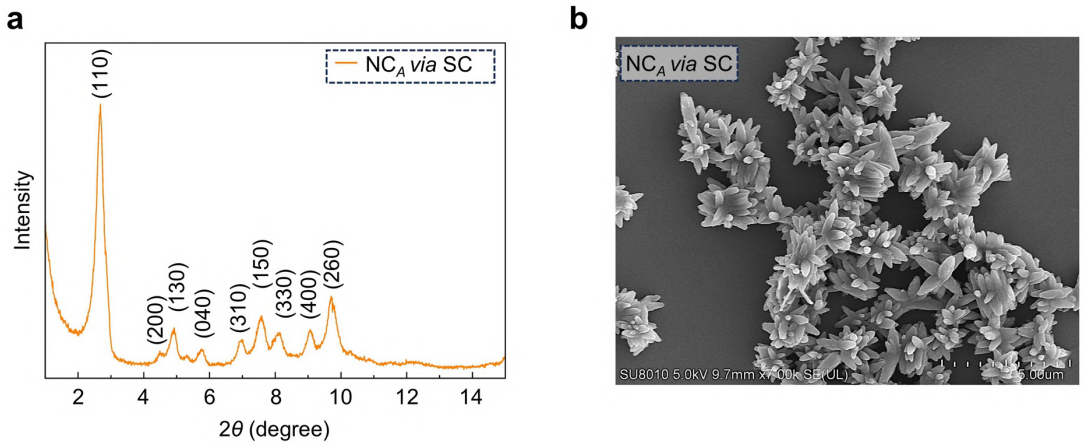

Supplementary Fig. 18 | a, PXRD pattern of **NC$_A$** recrystallized from DMF solution measured at 25 °C (Miller indices in parentheses). **b**, Representative SEM images of **NC$_A$** crystallites obtained from recrystallization in DMF solution.

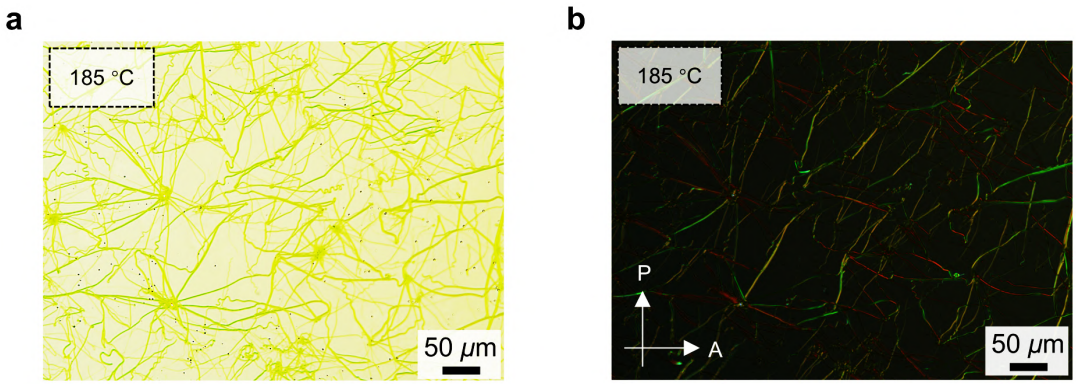

Supplementary Fig. 19 | **a**,**b**, OM (**a**) and POM (**b**) images of the reaction mixtures obtained by heating **NN**$_{rac}$ at 185 °C for 24 h. White arrows indicate the transmission axes of the polarizer (P) and analyzer (A).

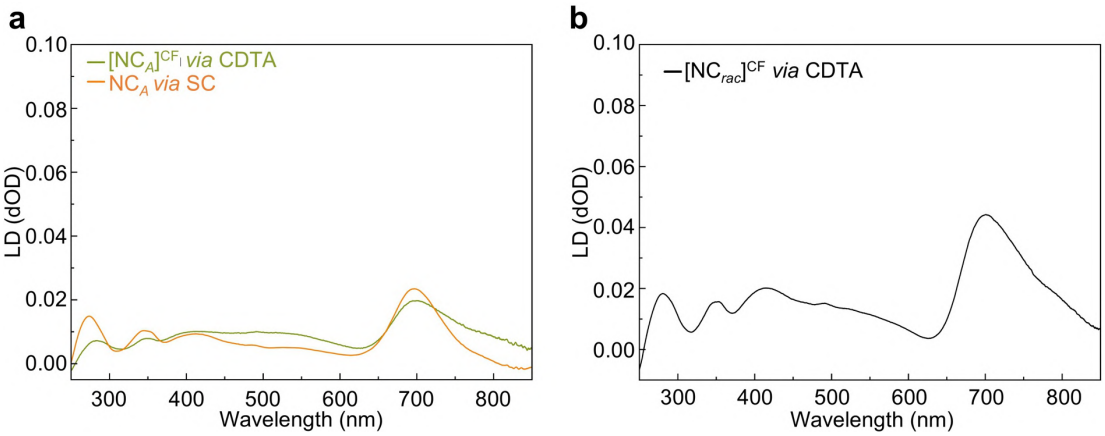

Supplementary Fig. 20 | **a**,**b**, LD spectra of the washed [**NC**$_A$]^{CF} (**a**, green), **NC**$_A$ crystallites (**a**, orange), and [**NC**$_{rac}$]^{CF} (**b**) suspensions in $CHCl_3$, obtained by CDTA and SC, respectively. Note that according to the references,[3,4] the equation representing the measured signals for circular and linear dichroism can be formulated as follow:

$$CD_{app} = CD + LD\cos 2\beta \sin\kappa + \frac{1}{6}[(CBLDLB - CDLB^2) + \left(\frac{1}{2}In10\right)^2 (CD^3 + CDLD^2)]$$

, where κ represents the static birefringence of the modulator, which is oriented at an angle β relative to the axis system of the induced birefringence.

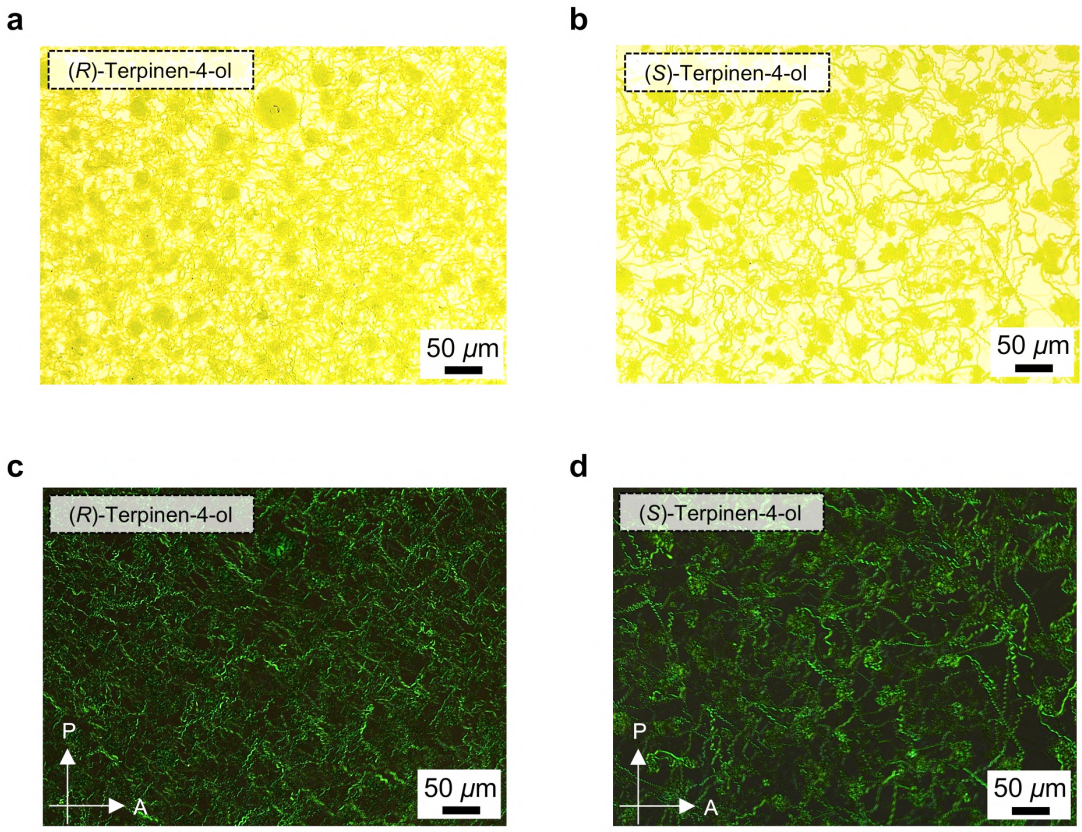

Supplementary Fig. 21 | **a**–**d**, OM (**a**,**b**) and POM (**c**,**d**) images of the reaction mixtures obtained by heating $\mathbf{NN}_A$ premixed with DCTH and (*R*)-Terpinen-4-ol (**a**,**c**) or (*S*)-Terpinen-4-ol (**b**,**d**) at a molar ratio of 6:1:1 at 185 °C for 12 h. White arrows indicate the transmission axes of the polarizer (P) and analyzer (A).

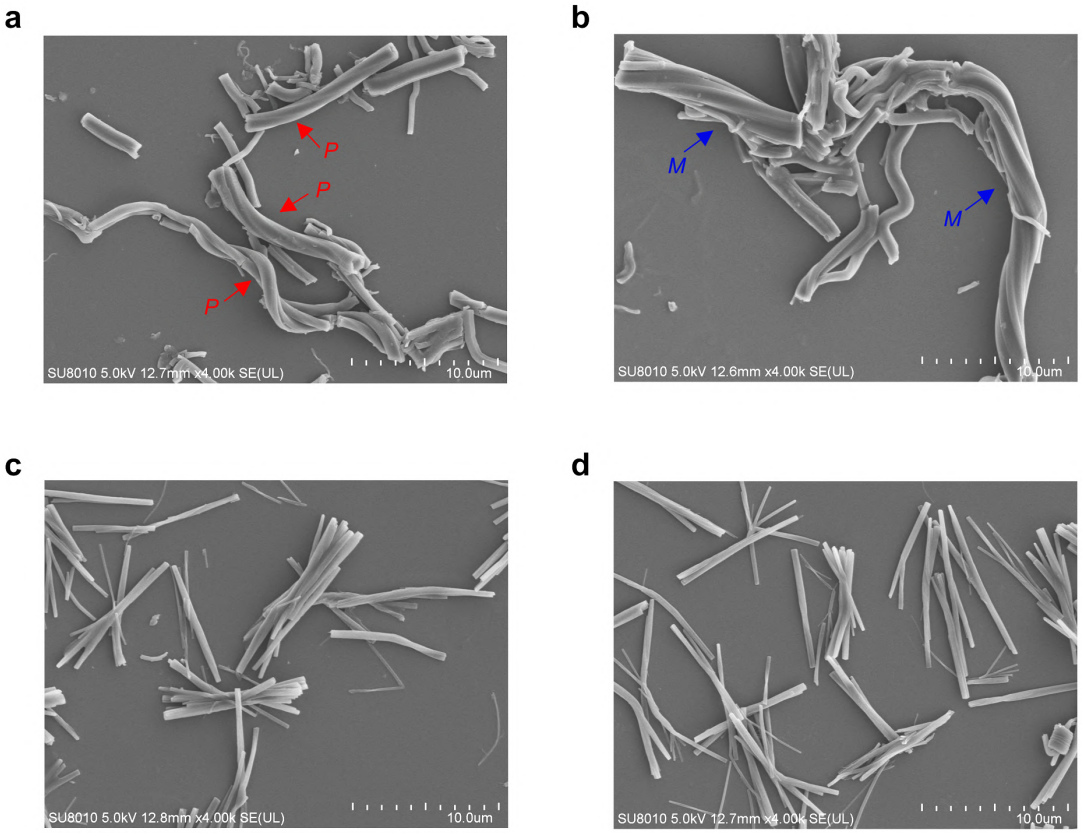

Supplementary Fig. 22 | **a**,**b**, Representative SEM images of *P*-helical $[\mathbf{NC}_{\boldsymbol{R}}]^{CF}$ (**a**) and *M*-helical $[\mathbf{NC}_{\boldsymbol{S}}]^{CF}$ (**b**) obtained by CDTA at 185 °C. **c**,**d**, Representative SEM images of $\mathbf{NC}_{\boldsymbol{R}}$ (**c**), and $\mathbf{NC}_{\boldsymbol{S}}$ (**d**) recrystallized from their DMF solutions.

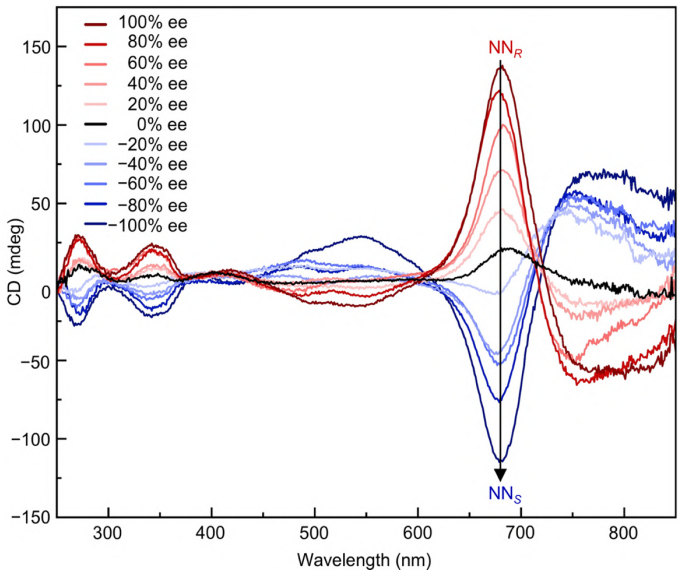

Supplementary Fig. 23 | CD spectra at 25 °C of $[NC]^{CF}$ suspensions in $CHCl_3$, obtained by CDTA of the reaction mixtures of $\mathbf{NN}_{\boldsymbol{R}}$ and $\mathbf{NN}_{\boldsymbol{S}}$ with different *ee* values upon heating at 185 °C for 12 h. The black line (*ee* = 0%) corresponds to $[\mathbf{NC}_{\boldsymbol{rac}}]^{CF}$, which is a 1:1 mixture of $\mathbf{NN}_{\boldsymbol{R}}$ and $\mathbf{NN}_{\boldsymbol{S}}$. The dark red (*ee* = 100%) and blue (*ee* = −100%) lines correspond to the pure $[\mathbf{NC}_{\boldsymbol{R}}]^{CF}$ and $[\mathbf{NC}_{\boldsymbol{S}}]^{CF}$, respectively.

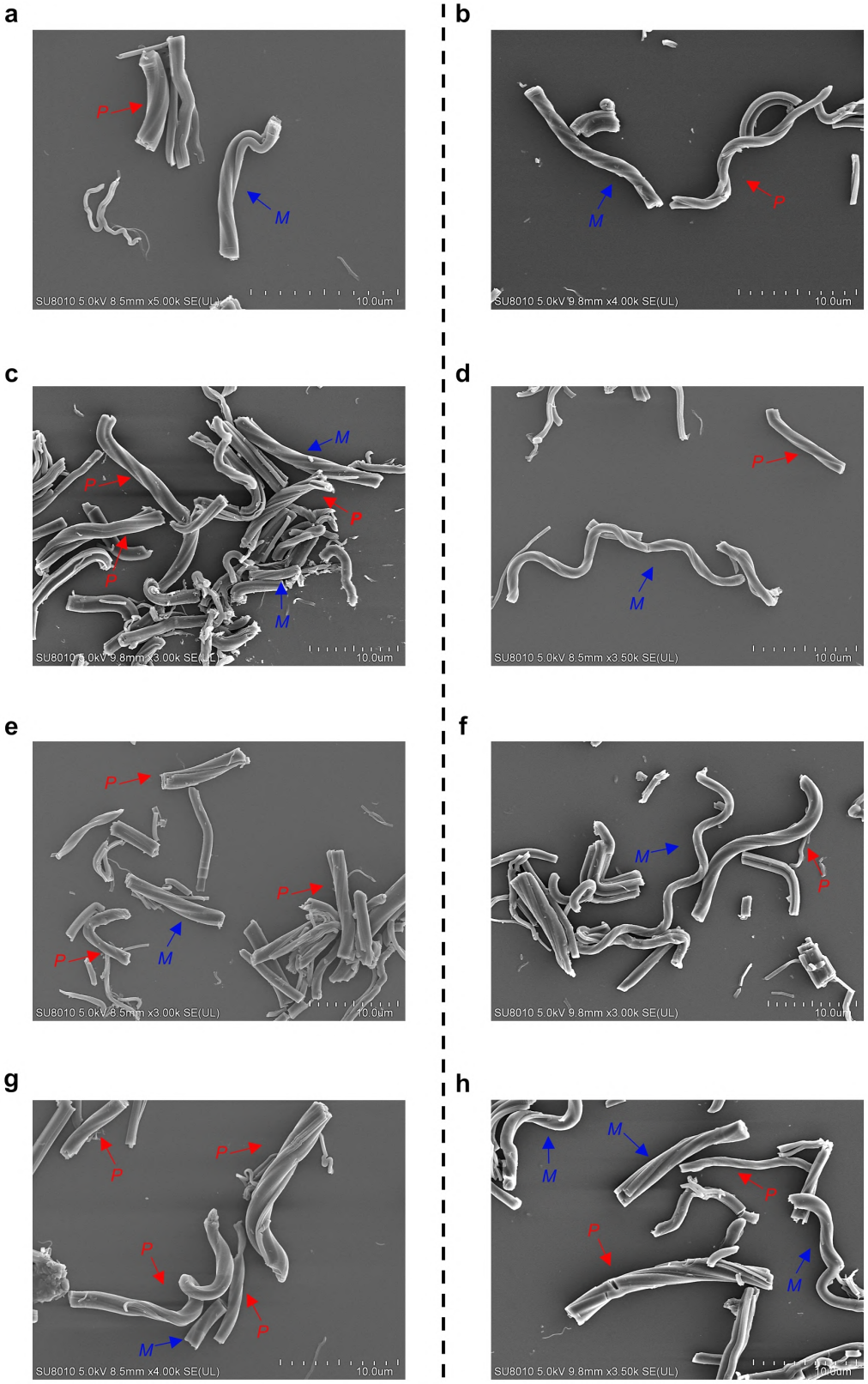

Supplementary Fig. 24 | **a**–**h**, Representative SEM images of the helical fibres obtained by CDTA of 80%-*ee* mixture of $\mathbf{NN}_{\boldsymbol{R}}/\mathbf{NN}_{\boldsymbol{S}}$ (9/1) (**a**), −80%-*ee* mixture of $\mathbf{NN}_{\boldsymbol{R}}/\mathbf{NN}_{\boldsymbol{S}}$ (1/9) (**b**), 60%-*ee* mixture of $\mathbf{NN}_{\boldsymbol{R}}/\mathbf{NN}_{\boldsymbol{S}}$ (8/2) (**c**), −60%-*ee* mixture of $\mathbf{NN}_{\boldsymbol{R}}/\mathbf{NN}_{\boldsymbol{S}}$ (2/8) (**d**), 40%-*ee* mixture of $\mathbf{NN}_{\boldsymbol{R}}/\mathbf{NN}_{\boldsymbol{S}}$ (7/3) (**e**), and −40%-*ee* mixture of $\mathbf{NN}_{\boldsymbol{R}}/\mathbf{NN}_{\boldsymbol{S}}$ (3/7) (**f**), 20%-*ee* mixture of $\mathbf{NN}_{\boldsymbol{R}}/\mathbf{NN}_{\boldsymbol{S}}$ (6/4) (**g**), and −20%-*ee* mixture of $\mathbf{NN}_{\boldsymbol{R}}/\mathbf{NN}_{\boldsymbol{S}}$ (4/6) (**h**) at 185 °C.

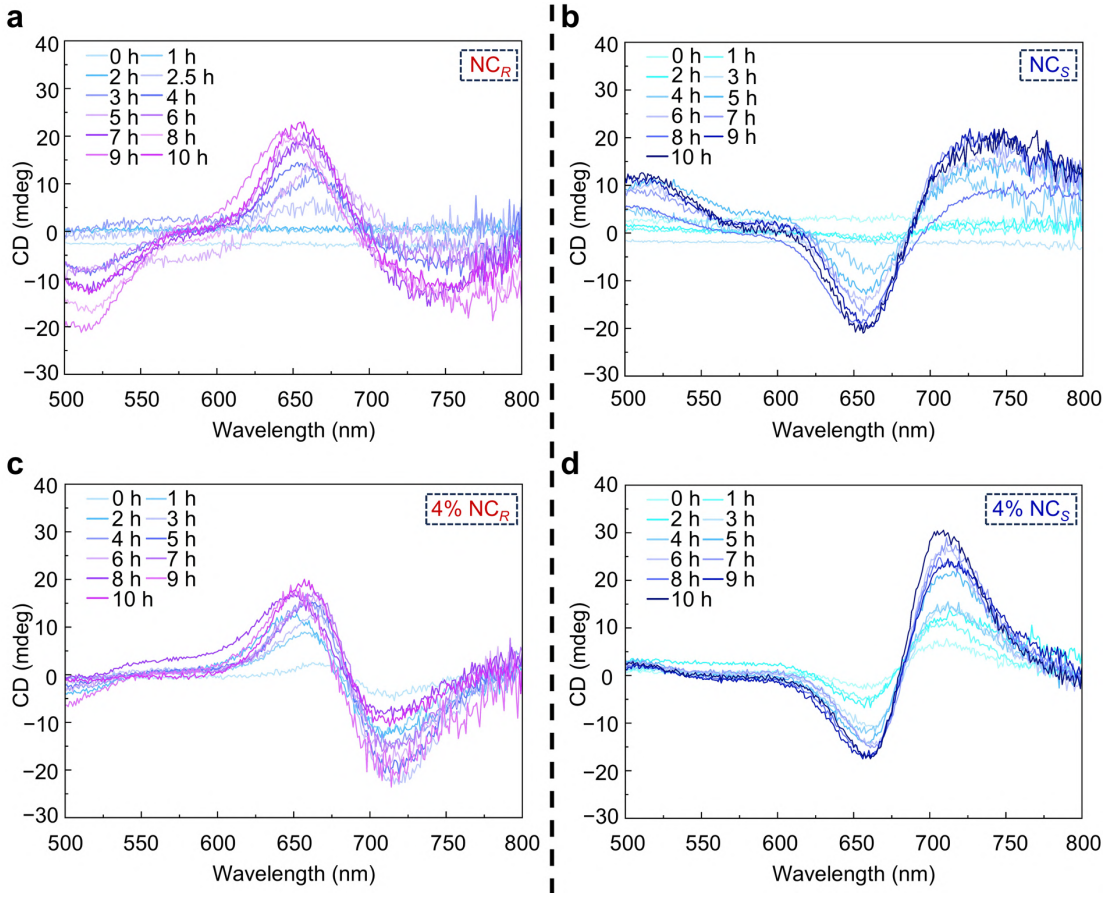

Supplementary Fig. 25 | **a**,**b**, CD spectra on glass substrates of the reaction mixtures obtained by CDTA of **NN**$_R$ (**a**) and **NN**$_S$ (**b**), upon heating at 185 °C for different time. **c**,**d**, CD spectra on glass substrates of the reaction mixtures obtained by seeded CDTA of **NN**$_A$ premixed with [**NC**$_R$]^{CF} (**c**) and [**NC**$_S$]^{CF} (**d**) as chiral seeds, upon heating at 185 °C for different time.

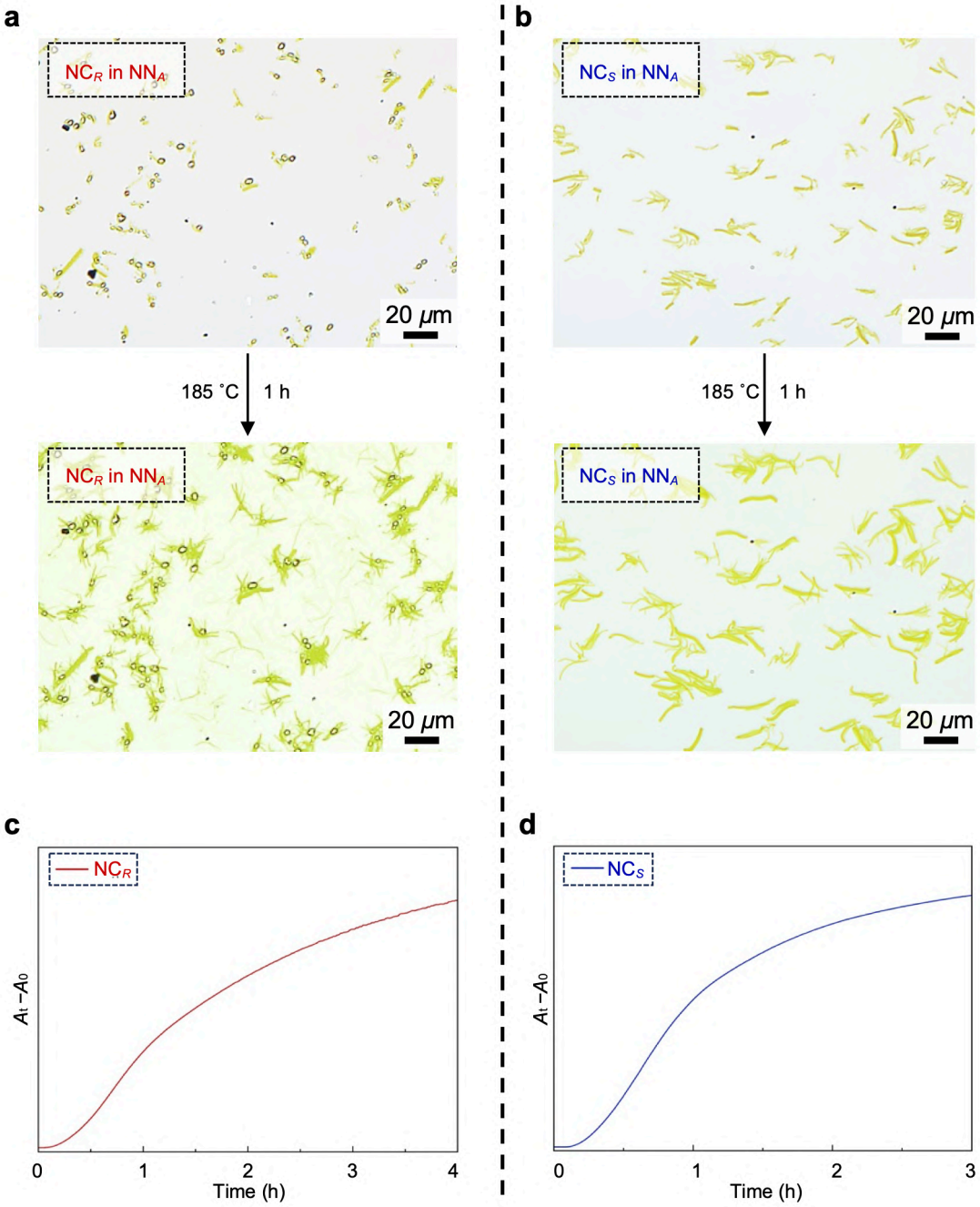

Supplementary Fig. 26 | **a**,**b**, OM images of the reaction mixtures obtained by seeded CDTA of $\mathbf{NN}_A$ premixed with $[\mathbf{NC}_R]^{CF}$ (**a**) and $[\mathbf{NC}_S]^{CF}$ (**b**) as chiral seeds (4 mol%), upon heating at 185 °C for 1 h. **c**,**d**, Time-dependent changes of absorption intensity at 810 nm of the reaction mixtures obtained by seeded CDTA of $\mathbf{NN}_A$ premixed with $[\mathbf{NC}_R]^{CF}$ (**c**) and $[\mathbf{NC}_S]^{CF}$ (**d**) as chiral seeds (4 mol%) upon heating at 185 °C.

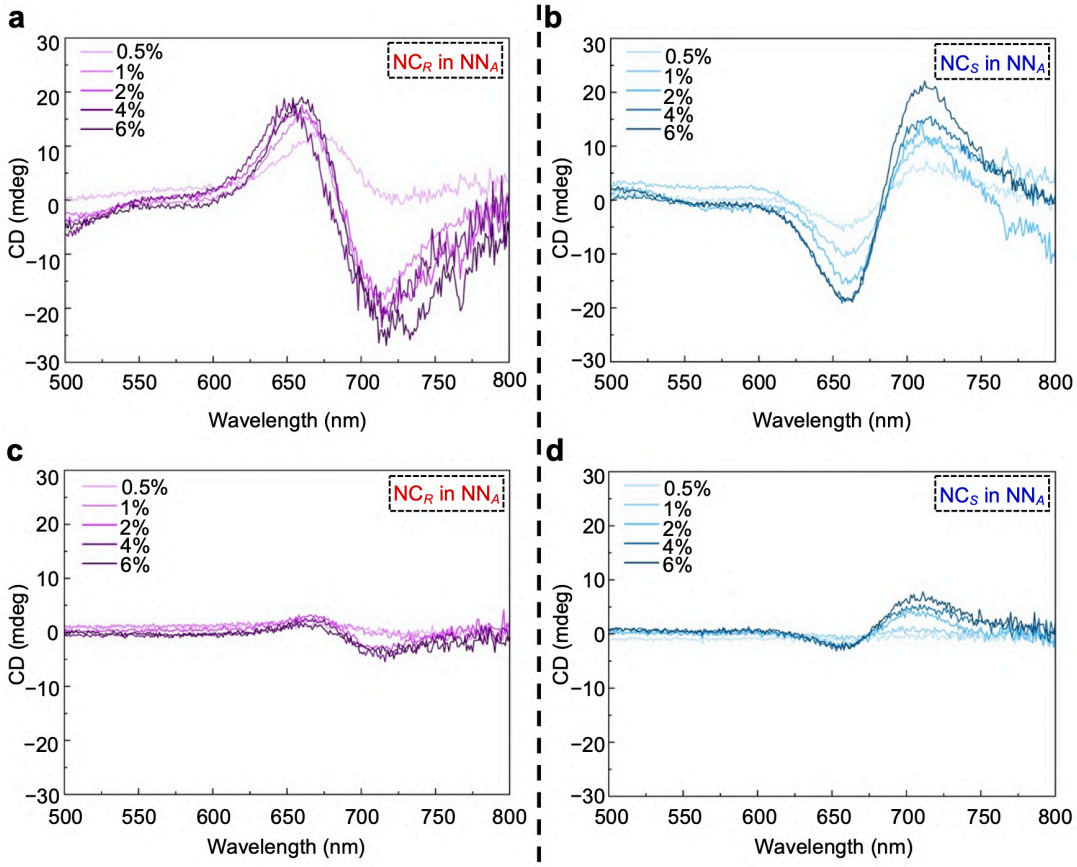

Supplementary Fig. 27 | **a**–**d**, CD spectra on glass substrates of the reaction mixtures obtained by seeded CDTA of **NN**$_A$ premixed with [**NC**$_R$]^{CF} (**a**,**c**) and [**NC**$_S$]^{CF} (**b**,**d**) as chiral seeds upon heating at 185 °C for 0 h (**c**,**d**) and 12 h (**a**,**b**).

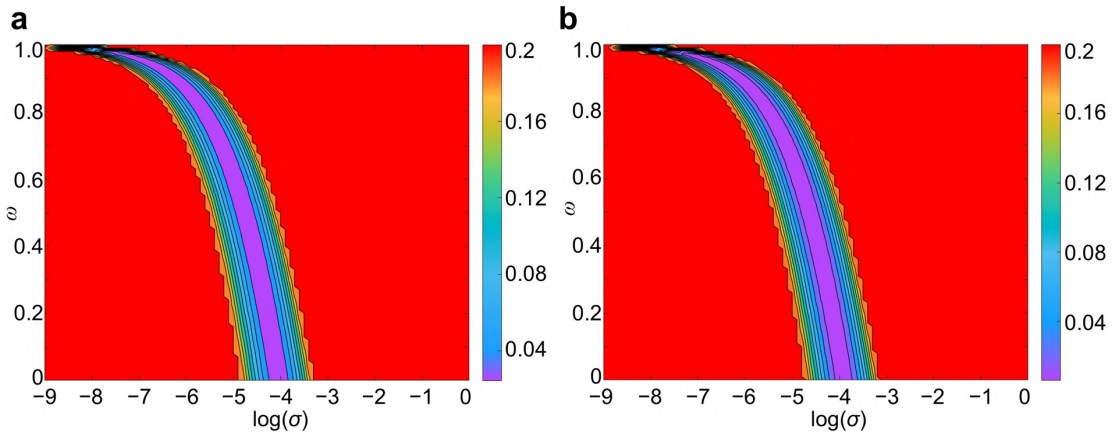

Supplementary Fig. 28 | **a**, Contour plot of the sum of squared residuals obtained from fitting Sergeant-and-Soldiers experimental data in %-molar fractions of $[\mathbf{NC}_{\boldsymbol{R}}]^{CF}$ with the minimum at which the dotted lines cross ($\sigma = 2.75 \times 10^{-6}$ and $\omega = 0.60$). **b**, Contour plot of the sum of squared residuals obtained from fitting sergeant-and-soldiers experiments of $[\mathbf{NC}_{\boldsymbol{S}}]^{CF}$ in different ratio data with the minimum at which the dotted lines cross ($\sigma = 2.2 \times 10^{-5}$ and $\omega = 0.64$).

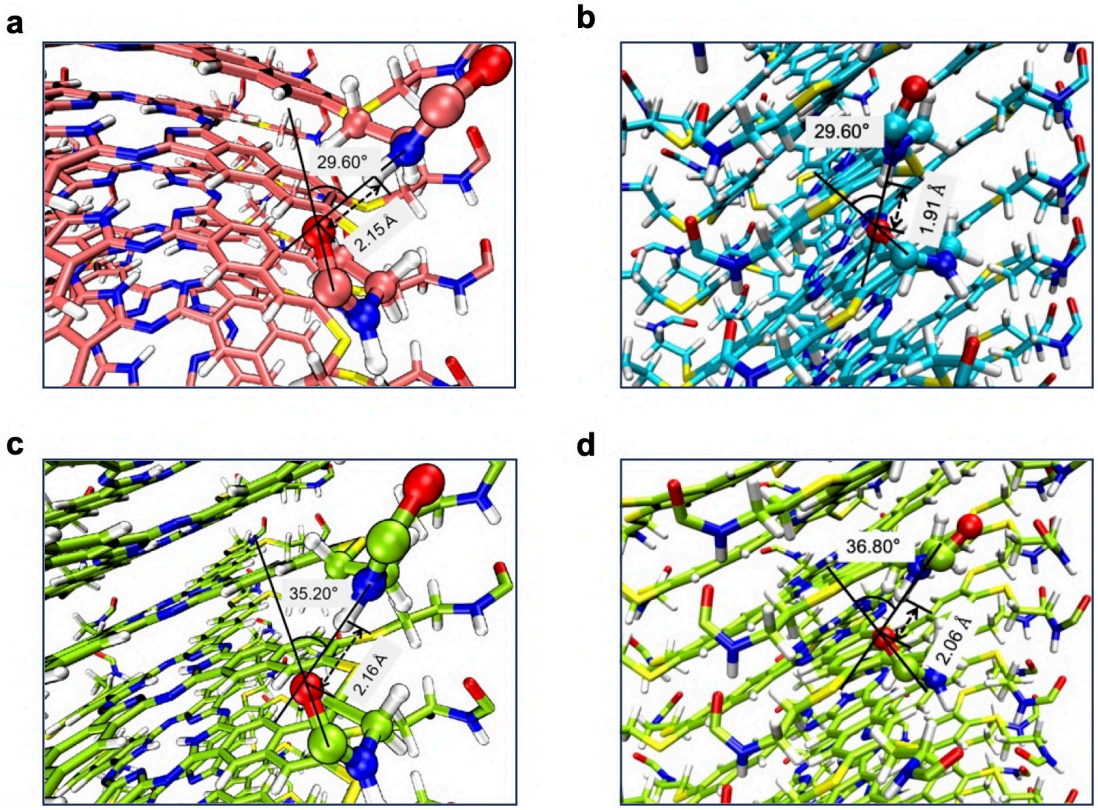

Supplementary Fig. 29 | **a**–**d**, Optimized CPK modes on the hydrogen-bonding conformation of amide groups in *P*-helical **NC**$_{R}$ (**a**) and *M*-helical **NC**$_{S}$ (**b**) as well as *P*-helical **NC**$_{A}$ (**c**) and *M*-helical **NC**$_{A}$ (**d**) columns.

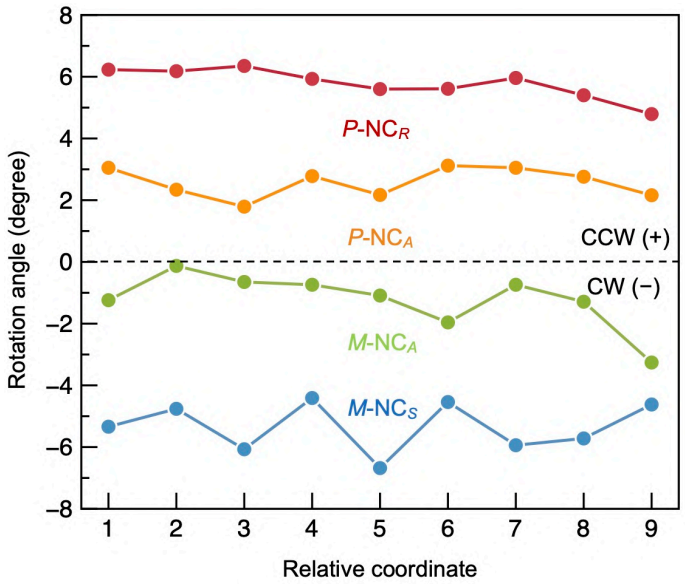

Supplementary Fig. 30 | Plot of the rotation angles between adjacent NC molecules along the columnar axis at different coordinates obtained by DFT calculations.

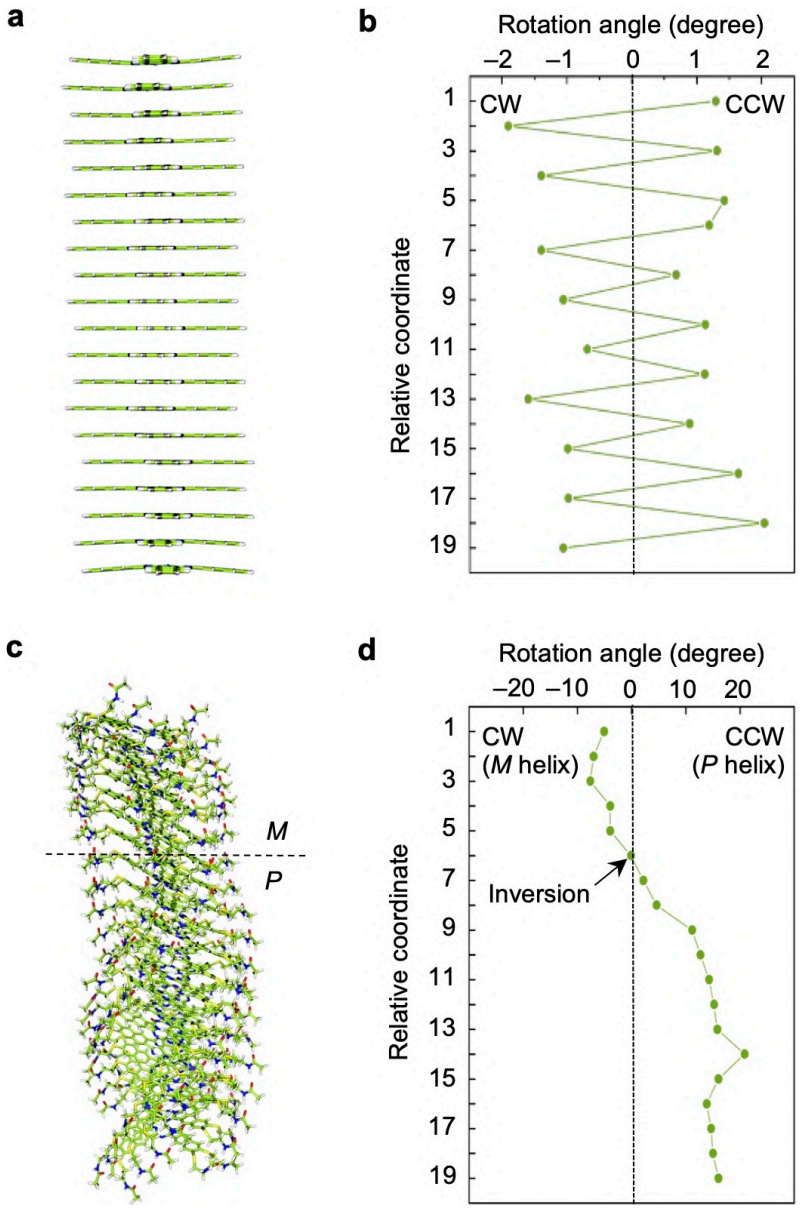

Supplementary Fig. 31 | **a**,**c**, The optimized geometries of supramolecular columns consisting of twenty NC molecules (**a**) and amide-tailored NC derivatives without side chains (**c**) based on the GFN2-xTB method. **b**,**d**, Plots of the rotation angles between adjacent NC molecules (**b**) and amide-tailored NC derivatives (**d**) along the columnar axis at different coordinates obtained by DFT calculations.

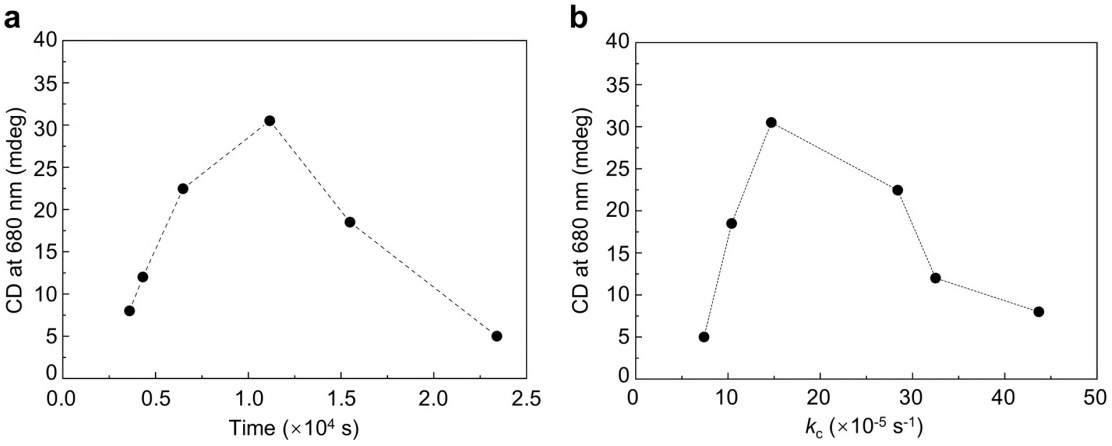

Supplementary Fig. 32 | **a,b** Plots of CD intensity at 680 nm versus nucleation time (**a**) and corresponding kinetic rate constants k_c (**b**). All reaction mixtures were prepared by heating **NN**$_A$ premixed with DCTH at molar ratios of 1:2, 1:1, 2:1, 3:1, 4:1, 5:1 at 185 °C for 12 h.

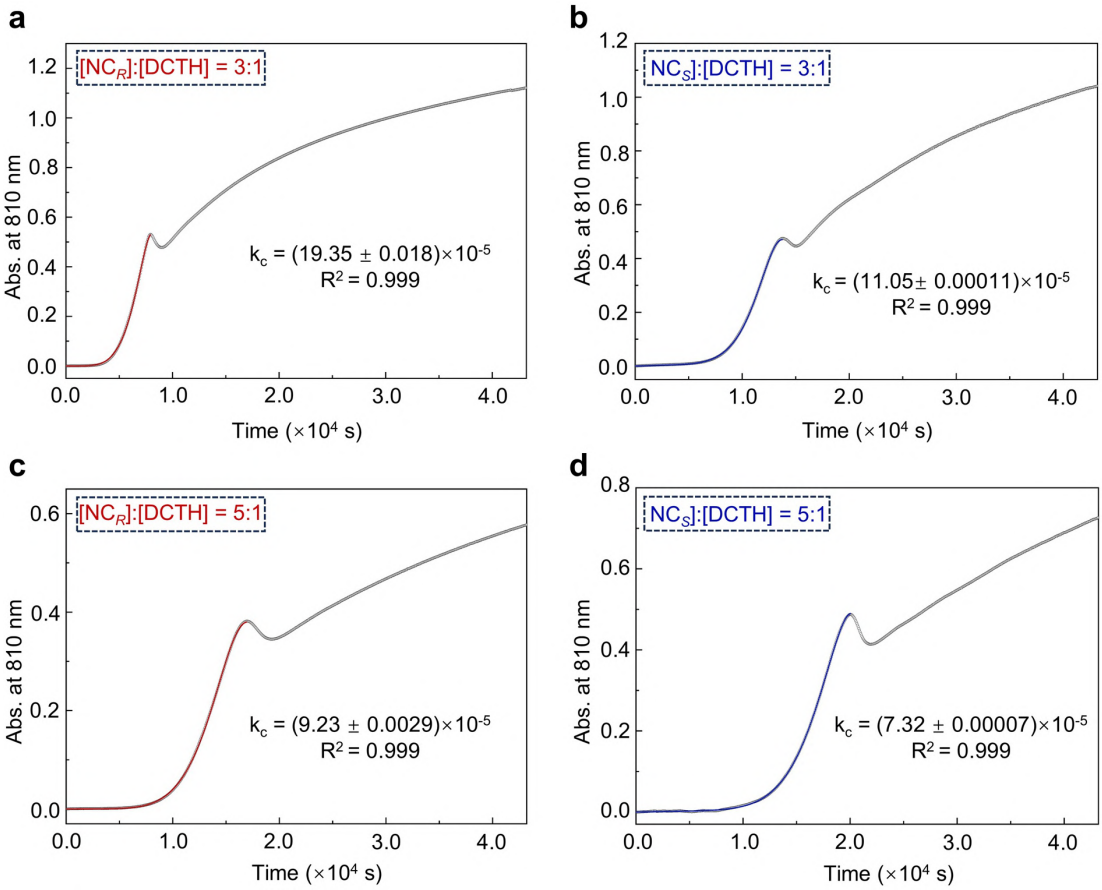

Supplementary Fig. 33 | **a**–**d**, Kinetic and fit profiles of absorbance for the reaction mixtures obtained by heating **NN*R*** (**a**,**c**) and **NN*S*** (**b**,**d**) premixed with DCTH at molar ratios of 3:1 (**a**,**b**) and 5:1 (**c**,**d**) at 185 °C for 12 h. The solid lines represent the fit ($R^2 = 0.999$) on an autocatalytic model in the nucleation stage of CDTA.

4. Supplementary Tables

Supplementary Table 1 | PXRD Data of $[NC_A]^{CF}$

$[NC_A]^{CF}$	2θ (degree)	$d_{obs.}$ (nm)	$d_{cal.}$ (nm)	*hkl*
$C2/m^a$	2.68	3.29	3.29	(110)
(25 °C)	4.56	1.94	1.95	(200)
	4.88	1.81	1.82	(130)
	5.37	1.65	1.65	(220)
	5.75	1.54	1.54	(040)
	7.01	1.26	1.27	(310)
	7.56	1.17	1.18	(510)
	8.12	1.09	1.10	(330)
	9.09	0.97	0.97	(400)
	9.76	0.91	0.91	(260)

[a]Orthorhombic lattice parameter: b = 6.16 nm, a = 3.90 nm

Supplementary Table 2 | PXRD Data of $[NC_R]^{CF}$

$[NC_R]^{CF}$	2θ (degree)	$d_{obs.}$ (nm)	$d_{cal.}$ (nm)	*hkl*
$C2/m^a$	2.68	3.30	3.30	(110)
(25 °C)	4.84	1.83	1.83	(130)
	5.36	1.65	1.65	(220)
	5.66	1.56	1.55	(040)
	7.05	1.25	1.26	(310)
	7.44	1.19	1.18	(150)
	8.4	1.05	1.09	(330)

[a]Orthorhombic lattice parameter: b = 6.20 nm, a = 3.89 nm

Supplementary Table 3 | PXRD Data of $[\mathbf{NC}_S]^{CF}$

$[\mathbf{NC}_S]^{CF}$	2θ (degree)	$d_{obs.}$ (nm)	$d_{cal.}$ (nm)	*hkl*
$C2/m^a$	2.68	3.30	3.30	(110)
(25 °C)	4.84	1.83	1.83	(130)
	5.36	1.65	1.65	(220)
	5.66	1.56	1.55	(040)
	7.05	1.25	1.26	(310)
	7.44	1.19	1.18	(150)
	8.4	1.05	1.09	(330)

[a]Orthorhombic lattice parameter: b = 6.20 nm, a = 3.89 nm

Supplementary Table 4 | PXRD Data of $\mathbf{NC}_A$ crystallites

$\mathbf{NC}_A$ (Crystallites)	2θ (degree)	$d_{obs.}$ (nm)	$d_{cal.}$ (nm)	*hkl*
$C2/m^a$	2.68	3.29	3.29	(110)
(25 °C)	4.56	1.94	1.95	(200)
	4.88	1.81	1.82	(130)
	5.37	1.65	1.65	(220)
	5.75	1.54	1.54	(040)
	7.01	1.26	1.27	(310)
	7.56	1.17	1.18	(510)
	8.12	1.09	1.10	(330)
	9.09	0.97	0.97	(400)
	9.76	0.91	0.91	(260)

[a]Orthorhombic lattice parameter: b = 6.16 nm, a = 3.90 nm

Supplementary Table 5 | Kinetic parameters in the nucleation stage of CDTA

[**NN**$_A$]/[DCTH]	nucleation time (s)	k_0 ($\times 10^{-6}$ s^{-1})	k_c ($\times 10^{-5}$ s^{-1})	CD (mdeg)
1/2	3600	0.00 ± 2.71	43.73 ± 0.15	8.0
1/1	4320	1.84 ± 0.23	32.15 ± 0.01	12.0
2/1	6480	0.00 ± 2.04	28.41 ± 0.11	22.5
3/1	11160	0.01 ± 0.29	14.72 ± 0.02	30.5
4/1	15480	0.89 ± 0.03	10.37 ± 0.01	18.5
5/1	23400	0.00 ± 0.11	7.39 ± 0.01	5.0

5. Captions of Supplementary Video

Supplementary Video 1 | *In-situ* OM observation on the CDTA of $[\mathbf{NC}_{A}]^{\mathbf{CF}}$

A powdered sample of $\mathbf{NN}_{A}$ was sandwiched with glass plates upon heating at 185 °C, during which yellow-green colored crystalline fibers formed. This video was recorded in a period of 0–8 h after heating. The fibers started to appear after 3 h and then developed entirely. This 24-second movie was prepared by 1200-time acceleration.

Supplementary Video 2 | *In-situ* OM observation on the CDTA of $[\mathbf{NC}_{R}]^{\mathbf{CF}}$

A powdered sample of $\mathbf{NN}_{R}$ was sandwiched with glass plates upon heating at 185 °C, during which yellow-green colored crystalline fibers formed. This video was recorded in a period of 0–6.6 h after heating. The fibers started to appear after about 2.9 h and then developed entirely. This 19-second movie was prepared by 1200-time acceleration.

Supplementary Video 3 | *In-situ* OM observation on the CDTA of $[\mathbf{NC}_{S}]^{\mathbf{CF}}$

A powdered sample of $\mathbf{NN}_{S}$ was sandwiched with glass plates upon heating at 185 °C, during which yellow-green colored crystalline fibers formed. This video was recorded in a period of 0–8.3 h after heating. The fibers started to appear after about 4.4 h and then developed entirely. This 24-second movie was prepared by 1200-time acceleration.

Supplementary Video 4 | Statistical analysis of the *P*- and *M*-type helices in $[\mathbf{NC}_{A}]^{\mathbf{CF}}$

The as-formed $[\mathbf{NC}_{A}]^{\mathrm{CF}}$ from different batches were suspended in chloroform and subjected to ultrasonication for uniform dispersion. The suspensions were then deposited onto silicon wafers, and after solvent evaporation, 50 photos of SEM images were collected. These photos were compiled into a 10-second video, with each frame displayed for 0.2 seconds, for visualization of the *P*- and *M*-type fibers for statistical analysis in number.

Supplementary Video 5 | Statistical analysis of the *P*- and *M*-type helices in $[\mathbf{NC}_{rac}]^{\mathbf{CF}}$

The as-formed $[\mathbf{NC}_{rac}]^{\mathrm{CF}}$ from different batches were suspended in chloroform and subjected to ultrasonication for uniform dispersion. The suspensions were then deposited onto silicon wafers, and after solvent evaporation, 50 photos of SEM images were collected. These photos were compiled into a 10-second video, with each frame displayed for 0.2 seconds, for visualization of the *P*- and *M*-type fibers for statistical analysis in number.

6. Supplementary References

1 Smulders, M. M. J. et al. Tuning the extent of chiral amplification by temperature in a dynamic supramolecular polymer. *J. Am. Chem. Soc.* **132**, 611–619 (2010).

2 Romeo, A. et al. Kinetic control of chirality in porphyrin *J*-aggregates. *J. Am. Chem. Soc.* **136**, 40–43 (2013).

3 Davidsson, Å. Measurement of oriented circular dichroism. *Chem. Phys. Lett.* **70**, 313–316 (1980).

4 Mineo, P., Villari, V., Scamporrino, E. & Micali, N. Supramolecular chirality induced by a weak thermal force. *Soft Matter* **10**, 44–47 (2014).